

1 **Late Holocene great earthquakes in the eastern part of the Aleutian megathrust**

2 Ian Shennan¹, Ronald Bruhn², Natasha Barlow¹, Kelly Good², Emma Hocking^{1,3}

3 ¹ *Sea Level Research Unit, Department of Geography, Durham University, Durham,*

4 *DH1 3LE, UK*

5 ²*Department of Geology and Geophysics, University of Utah, Salt Lake City, UT 84112-*

6 *0111, USA*

7 ³ *Current address: Department of Geography, Northumbria University, Newcastle upon*

8 *Tyne, NE1 8ST, UK*

9

10 **ABSTRACT**

11 The great earthquake, M_w 9.2, of AD 1964 may not be typical of other megathrust
12 earthquakes in the region during the last 4000 years. We present new field data from
13 three sites: Copper River Delta, the lower Katalla River valley and Puffy Slough, to
14 enhance the temporal and spatial resolutions of the paleoseismic records of multiple
15 great earthquakes. Differences in the spatial patterns of coseismic uplift and
16 subsidence suggest different rupture combinations of the Kodiak, Prince William Sound
17 and western Yakutat segments of the plate boundary. The longest and most
18 comprehensive records all come from the Prince William Sound segment. Most sites
19 here reveal net subsidence over multiple earthquake cycles except where probable
20 upper plate faulting contributes locally to net uplift, with measurable differences between
21 sites only a few kilometers apart. We identify the Katalla area as a source of local
22 seismic hazard, similar to other locations in the western part of the Yakutat microplate,
23 including the two M_w8+ ruptures in AD 1899. We use a Bayesian radiocarbon modeling

24 approach to estimate the age and recurrence intervals of multiple great earthquakes for
25 the Prince William Sound segment of the megathrust. The long interval, 883 ± 34 (2σ)
26 years, between the penultimate earthquake and AD 1964 contrasts with the older
27 earthquakes that have intervals ranging from ~ 420 to ~ 610 years, with a mean of ~ 535
28 years.

29

30

31 **1. INTRODUCTION**

32 Paleoseismological investigations provide both major inputs and challenges for seismic
33 hazard assessment. While the classic notion of the characteristic earthquake, with
34 constant dimensions and recurrence interval over multiple earthquake cycles, forms the
35 basis for the time-independent seismic hazard maps of Alaska (Wesson et al., 2007),
36 the growth of paleoseismological studies and improvements in analytical methods (Boyd
37 et al., 2008) raise fundamental questions that require further analysis, including
38 segmentation and magnitude-frequency relationships (Wesson et al., 2008). The great
39 Alaskan earthquake, $M_w 9.2$, of March 1964, ruptured ~ 950 km of the Aleutian
40 megathrust, encompassing the Kodiak and Prince William Sound segments (Carver and
41 Plafker, 2008), and resulted in coseismic uplift adjacent to the trench and a zone of
42 subsidence to the north and northwest (Figure 1).

43

44 Coastal marshes can register coseismic vertical land motions through changes in
45 sediment lithology and biostratigraphy, providing records of 1964 and previous great
46 earthquakes. The latest of these occurred ~ 500 years ago and ruptured only the Kodiak

47 segment (Carver and Plafker, 2008), while correlation of radiocarbon ages suggest
48 earlier great earthquakes involved either multi-segment ruptures or closely timed
49 sequences of single segment ruptures (Carver and Plafker, 2008; Hutchinson and
50 Crowell, 2007; Shennan et al., 2009). The longest records come from the eastern part
51 of the Prince William Sound segment, at Copper River Delta, with ten great earthquakes
52 since ~5000 cal yr BP (Carver and Plafker, 2008). Farther east, uplifted coastal
53 sediments suggest that earthquakes ~900 and ~1500 years ago may have
54 simultaneously ruptured adjacent segments of the Aleutian megathrust and the Yakutat
55 microplate (Shennan et al., 2009).

56

57 Here we use new field data from Copper River Delta, the lower Katalla river valley and
58 Puffy Slough (Figure 2) to enhance the temporal and spatial resolutions of the
59 paleoseismic records of multiple great earthquakes. We provide a new synthesis and
60 temporal model of earthquake recurrence through the Late Holocene using the
61 Bayesian modeling approach outlined by Lienkaemper and Bronk Ramsey (2009) and
62 aim to explain variations in the spatial pattern of coseismic deformation between sites
63 during the Late Holocene.

64

65 **2. FIELD AND LABORATORY METHODS**

66 In analyzing coastal sediment sequences, four critical criteria help determine a co-
67 seismic signal and discriminate from non-seismic processes that might cause abrupt
68 wetland submergence or emergence: lateral extent of peat-mud couplets with sharp
69 contacts; suddenness of subsidence or emergence; amount of vertical motion; and

70 synchronicity with other sites (Nelson et al., 1996). Presence of tsunami sediments may
71 also help in certain geographical settings. We use exposures and sediment cores to
72 assess the lithological evidence for these criteria, diatom-based transfer function
73 models to quantify the vertical motion, and AMS radiocarbon dating of *in situ*
74 herbaceous macrofossils to provide a chronology for each site. For the transfer function
75 models we use a regional-scale modern training set collected from a wide range of
76 marshes across ~1000 km of south central Alaska in order to seek the best fit between
77 fossil and modern diatom assemblages (Watcham et al., 2013). We use three models,
78 constrained by the lithology of the Holocene sediment sequence (Table 1); one for peat
79 sediment, a second for silt units with visible plant rootlets and a third for silt units with no
80 rootlets (Hamilton and Shennan, 2005). We assess goodness of fit between each
81 fossil sample and the modern dataset using a dissimilarity coefficient, using the 20th
82 percentile of the dissimilarity values for the modern samples as the cut-off between
83 'close' and 'poor' modern analogues for fossil samples, and the 5th percentile as the
84 threshold for defining 'good' modern analogues (Hamilton and Shennan, 2005). For
85 reconstructions of the elevation at which the fossil sediment was laid down, termed
86 paleo marsh surface elevation, we present sample-specific 95% error terms.

87

88 **3. NEW FIELD DATA**

89

90 **3.1 Copper River Delta**

91 During the 1964 earthquake the delta was raised on the order of 2 to 3 m (McCalpin and
92 Carver, 2009; Plafker, 1969). Previous investigations record up to nine pre-1964

93 earthquakes, revealed by multiple couplets of silt overlain by peat, representing
94 coseismic uplift of intertidal mud flats, colonization by freshwater marshes, and gradual
95 interseismic subsidence (Carver and Plafker, 2008; Plafker et al., 1992). The vertical
96 sequence of couplets seen in cores, some more than 11 m in depth, and sections
97 indicates net submergence over multiple earthquake cycles, i.e. the sum of non-seismic
98 relative sea-level change (glacio-isostasy and eustasy), sediment compaction and inter-
99 seismic subsidence is greater than coseismic uplift.

100

101 Two pre-1964 silt-peat sequences are widely exposed in the uppermost ~4 m of the
102 delta sediments exposed along tidal channels (Figure 3) but correlation of some of the
103 older couplets recorded from coring is problematical (Carver and Plafker, 2008). Our
104 primary aim of collecting new material from Copper River Delta was to obtain estimates
105 of the coseismic uplift for different Late Holocene earthquakes. We sampled at three
106 locations along an 8 km stretch of Alaganik Slough (Figure 4), one of the tributaries in
107 the delta west of the main river, using exposures and cores to establish the lateral
108 continuity of each silt-peat couplet in the field.

109

110 Our diatom analyses highlight a key challenge of reconstructing land-level changes in
111 this large delta. We found highly variable diatom preservation in the silt units. For each
112 silt-peat couplet sampled and dated (Table 2) we could count sufficient diatoms in the
113 silt unit to at least confirm formation within an intertidal environment but about half of the
114 samples had insufficient numbers to reach the minimum sum, 200, that we consider
115 suitable for quantitative analysis. We believe one of the major controls on diatom

116 abundance in tidal silt is the very high sediment concentration of the Copper River, the
117 delta and adjacent coastal waters. Of the surface samples we collected from Copper
118 River Delta to contribute to the modern training set described above, 14 of the 26 that
119 came from unvegetated tidal flat contained insufficient diatom numbers to reach the
120 minimum count so it is perhaps not unexpected to encounter similar limitations with
121 fossil sequences.

122

123 The most complete records are for the youngest pre-1964 silt-peat couplet, sampled at
124 all three sites. Diatom assemblages (Figure 4) record the greatest changes in salinity at
125 the most seaward site, 3, with lesser changes progressively upstream, as expected
126 where the influence of freshwater discharge becomes more dominant. At site 3 the
127 transfer function model estimates coseismic uplift ~ 1.3 m (Figure 5), at site 2 it is in the
128 order of 0.5 m, but with overlapping error terms, and at site 1 there is no clear change in
129 elevation. This may reflect the true pattern of differential uplift but it may also reflect the
130 increasing importance of river discharge as the controlling variable in sedimentation with
131 increasing distance from the open coast. For example, had we only studied this couplet
132 in the area around site 1 we would not be able to satisfy the demonstrable vertical
133 motion criterion outlined by Nelson et al. (1996) for attributing a couplet to a great
134 earthquake. In large coastal systems we recognize that certain areas will be sensitive
135 recorders of rapid emergence or submergence whereas other parts of the system are
136 relatively insensitive, as other parameters become more important controls on
137 sedimentation.

138

139 The radiocarbon age for the peat-silt couplet at site 1 also illustrate the limitations of
140 dating just the base of the peat unit as there may be a hiatus following uplift before plant
141 colonization and peat accumulation. It is preferable to bracket the event horizon with
142 two or more dated samples (Carver and Plafker, 2008; Shennan et al., 2009).

143

144 Low diatom abundances prevent us obtaining quantitative reconstructions for the older
145 couplets, except for the middle peat at site 3, where estimated uplift is ~1.1 m. We note
146 that the samples from this peat have poor modern analogues but their reconstructed
147 elevations are very similar to all the other samples from peat layers (Figure 5). In a
148 following section we consider this issue further alongside others that may complicate
149 the reconstruction of coseismic uplift.

150

151 **3.2 Katalla River Valley**

152 The Ragged Mountain Fault is located along the west side of the Katalla valley and
153 marks the western edge of the Yakutat Microplate (Figure 1). At the mouth of the Katalla
154 River, coseismic uplift of 1 to 3 m in 1964 raised the tidal marshes in the lee of a
155 vegetated storm ridge above the elevation of storm tides (McCalpin and Carver, 2009;
156 Plafker, 1969). Numerous prominent ridges occur upstream with low lying marshes
157 between them (Figure 6). Strata within the marshes record a Late Holocene archive of
158 net coastal progradation and relative land and sea-level change driven by repeated
159 cycles of coseismic uplift, interseismic relative sea-level rise/land subsidence, glacio-
160 isostasy and eustasy (McCalpin and Carver, 2009; Plafker, 1969; Richards, 2000; Sirkin
161 and Tuthill, 1971). A silt horizon, at river level and ~7 m above mean sea level

162 (Richards, 2000; Sirkin and Tuthill, 1971) contains mollusc species indicative of
163 intertidal conditions and dated to ~7 ka BP. Assuming a tidal range similar to present
164 (MHHW ~+1.55 m MSL and HAT ~2.65 m MSL), the mollusc bed indicates at least 4.35
165 m relative uplift over the past 7000 years. Sirkin and Tuthill (1971) indicate even older
166 marine deposits, >14 ka BP, may occur further up the valley.

167

168 The marsh stratigraphy between the ridges in the lower valley (Figure 6) provides
169 evidence of five episodes of coseismic uplift prior to 1964. The oldest is a minimum
170 limiting age of ~2650 – 2350 cal yr BP obtained from the base of peat overlying silt, in
171 marsh 5, location 5.3 (Figure 6). None of the samples contained sufficient diatom
172 abundances to provide quantitative reconstructions but the species present across this
173 abrupt silt-peat couplet, which could be traced laterally in a series of cores, indicate
174 freshwater marsh developed on uplifted intertidal sediment. The gradual transition up
175 the core from peat to silt indicates relative sea-level rise and return to intertidal
176 sedimentation. The same location records a second cycle of coseismic uplift, minimum
177 limiting age, ~2120 – 1950 cal yr BP, and interseismic relative sea-level rise.

178

179 We infer the next uplift event from the incision of intertidal/subtidal sand that is abruptly
180 overlain by lagoon mud at location 3.1, dated ~1510 – 1340 cal yr BP. Plant
181 macrofossils within the top of the silt unit and the base of the surface peat of marshes 3,
182 4 and 5 bracket the next earthquake horizon between 1120 – 960 cal yr BP and the
183 three minimum ages 930 – 790, 790 – 690 and 760 – 680 cal yr BP (Figure 6). Diatom
184 abundances were low in most samples across each of these silt-peat contacts; only that

185 from location 3.1 containing sufficient numbers to allow quantitative reconstructions of
186 elevation. Frequencies of individual species and the salinity summary classes show a
187 distinct change across the contact (Figure 7), with possibly some mixing within the top 2
188 cm of the silt horizon. Transfer function reconstructions indicate uplift in the order of 0.5
189 to 1 m between the silt and peat samples with close modern analogues while the two
190 samples from the top of the silt have poor modern analogues. We discuss further the
191 evidence for potential sediment and diatom mixing in a later section.

192

193 The final earthquake horizon is the contact between a subsurface peat and intertidal
194 sand that lies below the intertidal flat deposits that were uplifted in 1964 to become
195 freshwater marsh behind the prominent pre-1964 dune ridge (Figure 6). Samples from
196 two cores 2.5 km apart give minimum ages of 550 – 500 and 510 – 310 cal yr BP for
197 coseismic uplift, followed by freshwater marsh developed on raised intertidal sediment
198 surface, then relative sea-level rise and return to intertidal sedimentation in the tidal inlet
199 seen on pre-1964 aerial photographs (Figure 6b).

200

201 In summary, the record at Katalla shows a complicated interaction of multiple
202 earthquake cycles, with coseismic uplift and interseismic submergence, superimposed
203 on coastal progradation and non-seismic sea-level change. The net effect of eustasy
204 and glacio-isostasy is poorly understood for the area. While we see net relative uplift
205 over the past 7000 years, from the mollusc bed (Figure 6), the silt-peat couplets at site
206 3.3 are much closer to the formation elevations we get from the transfer function
207 estimates for peats at both Katalla and Copper River Delta, ~0.5 to 1m above MHHW.

208 Therefore net uplift over the last 2500 years is very small. In contrast, the peat-silt
209 contact dated by minimum ages ~700 to 900 years ago at sites in three of the marshes
210 (Figure 6) is well above the modern formation elevation, indicating recent net uplift.
211 This may relate to a different seismic source for the most recent pre-1964 earthquake,
212 recorded ~500 cal yr BP at sites in marsh 2, which we discuss further in the discussion
213 section below.

214

215 **3.3 Puffy Slough**

216 Preliminary investigations of exposed sections and cores at Puffy Slough, an intertidal
217 tidal marsh pre-1964, east of the Don Millar Hills and 2 to 5 km east of the Katalla sites,
218 reveal >6 m of silt with up to three silt-peat couplets, all with sharp lower contacts and
219 gradational upper contacts. These suggest at least three episodes of rapid uplift
220 separated by gradual submergence (Figure 6d). With only seven cores taken across
221 the marsh and low diatom counts in the silt units we simply note that the site appears to
222 record a paleoseismic record with net submergence over multiple earthquake cycles,
223 resulting from the combination of seismic and non-seismic land and sea-level change.
224 The record at Puffy Slough contrasts with Katalla in at least two key respects. First, the
225 absence of evidence for the earthquake and uplift recorded in marsh 2 at Katalla, dated
226 ~500 cal yr BP. Second, the youngest pre-1964 couplet, minimum age 760 – 670 cal
227 yr BP, at Puffy Slough is at a lower elevation than the equivalent contact at Katalla,
228 where it is at the base of the surface peat and not recording net submergence reverting
229 to intertidal sedimentation.

230

231

232 **4. QUANTIFYING COSEISMIC UPLIFT**

233 Whereas coseismic subsidence may result in a peat-silt couplet, caused by
234 submergence of freshwater marsh and rapid sedimentation of intertidal minerogenic
235 deposits commencing hours to weeks after the earthquake (Atwater et al., 2001), peat
236 formation on uplifted intertidal mudflat will not be instantaneous. There will be a time-
237 lag before the colonization of the exposed sediment surface by terrestrial plant
238 communities. Therefore, as noted above, we treat radiocarbon dates from the base of
239 the peat as minimum ages for the earthquake. Diatom analyses across the silt-peat
240 contacts from Katalla revealed a common phenomenon of mixed salinity assemblages
241 in the upper part of the silt unit. In some cases it was limited to the single sample at the
242 contact (Figure 7), but in others it extended further (Figure 8). At Katalla 5.5 we see a
243 peak of *Tabellaria flocculosa* across the silt-peat contact, commencing ~4cm below the
244 base of the peat. *T. flocculosa* is a freshwater species most commonly found attached
245 to the submerged stems of littoral species of sedges and reeds (Knudson, 1954; Patrick
246 and Reimer, 1966). We interpret this as evidence of ponding of freshwater on the
247 surface of the uplifted tidal flat, now above the limit of tidal inundation. Diatoms can
248 colonise and grow within a few weeks, therefore reflecting the environment following
249 uplift but before colonization by terrestrial plants. During this time we may expect
250 redistribution of surface sediment by a variety of processes, including rain, wind, surface
251 water flow and winter ice freeze-thaw. Where this occurs the redeposited silt with
252 freshwater diatoms does not represent the pre-earthquake environment and elevation.
253 At Katalla 5.5 low diatom counts prevent us taking this analysis further but it may be that

254 the base of the visibly coarser layer at 102 cm (Figure 8 and 9) is the earthquake
255 horizon, overlain by 5 cm of reworked silt with mix of diatoms from two main sources;
256 those already in the silt and those growing during the period of sediment reworking and
257 deposition. We have seen comparable evidence for similar sequences of events
258 between the time of uplift and peat formation at other sites. Figure 10c shows a box
259 sample from a tidal exposure at Copper River Delta that we declined to analyse further
260 as we could not trace the lateral continuity of the coarse layer more than a few meters in
261 the time available during the fieldwork. Mixed diatom assemblages below the modern
262 peat on the marsh at Cape Suckling uplifted in 1964 (Shennan, 2009) may also be the
263 result of sediment reworking on the uplifted surface prior to peat growth.

264

265 In summary, up to four factors may combine to make it probable that reconstructions
266 based on sediment and diatom stratigraphies will give minimum estimates of both the
267 age of a Holocene earthquake and the amount of coseismic uplift. First, there is the
268 time interval between uplift and peat accumulation. Second, there may be sediment
269 reworking at the top of the silt unit so it may be difficult to establish the pre earthquake
270 paleo surface elevation; mixing of tidal flat and purely freshwater diatom communities
271 would produce a too high estimate. Third, there will be initially rapid post-seismic
272 subsidence during the time interval between uplift and peat accumulation. For example,
273 at Cordova, only a few kilometers west of Copper River Delta, following uplift in 1964,
274 the tide gauge shows ~20 cm sea-level rise 1964 to 1979 and ~ 5 cm further rise 1979
275 to 2012 (NOAA, 2013). Finally, ground shaking of the unconsolidated tidal flat sediment

276 column during the earthquake may cause compaction and dewatering of unconsolidated
277 sediment and surface lowering.

278

279 **5. AGE MODELLING**

280 The OxCal Bayesian modeling approach outlined by Bronk Ramsey and Lienkaemper
281 (Bronk Ramsey, 2009; Lienkaemper and Bronk Ramsey, 2009) determines the best-fit
282 ages and recurrence intervals of multiple great earthquakes. It allows us to combine the
283 ages on earthquake horizons from all sites across the Prince William Sound segment,
284 whether they record coseismic uplift or coseismic subsidence. This a fundamental
285 difference to previous studies which first determine the chronology at each site, then
286 compare the patterns between sites (Carver and Plafker, 2008; Shennan and Hamilton,
287 2006).

288

289 This new approach assumes that the dated indicators of uplift or subsidence are either
290 minimum or maximum ages on the earthquake horizon. For coseismic subsidence,
291 maximum ages come from a peat contact below an intertidal silt unit and minimum ages
292 from samples within the silt unit. For coseismic uplift, maximum ages come from the top
293 part of intertidal silt below peat, and minimum ages from the peat (e.g. Figures 4 and 6).

294

295 Previous studies from Cook Inlet demonstrated the potential of contamination of bulk
296 peat samples by older carbon, such as coal deposits in the catchment (Hamilton et al.,
297 2005), so we exclude bulk peat samples from that area. With many bulk peat dates
298 available for other areas, particularly the key record from Copper River Delta published

299 previously (Carver and Plafker, 2008) we compared ages using bulk peat and AMS
300 dated samples on in situ plant macrofossils from the same locations. Whereas we see
301 major differences in the ages of the paired samples for sites around Cook Inlet we find
302 no significant differences for the four from Copper River Delta (Figure 10). Therefore
303 we include bulk peat ages from Copper River Delta in our analysis, but only ages for
304 samples of macrofossils at all other sites.

305

306 The OxCal Bayesian model seeks to estimate the age of each earthquake that is
307 bracketed by dated samples assuming no knowledge of sedimentation rate pre- or post-
308 earthquake. Samples are grouped into “*phases*”, where one *phase* is all the samples
309 giving a minimum age on earthquake n , and another *phase* will be all the maximum
310 ages for earthquake n (Lienkaemper and Bronk Ramsey, 2009). There is no
311 chronological ordering within a *phase*, but the stratigraphic ordering of phases and
312 earthquake horizons is a powerful constraint (Figure 11a). Our full model uses 9 pre-
313 historic earthquakes of unknown age and the 1964 earthquake as a known boundary.
314 We exclude the ~ 500 cal yr BP earthquakes at Kodiak and Katalla as we have no
315 evidence for them rupturing other parts of the 1964 rupture zone. Between each pair of
316 earthquakes we have two *phases*, assuming the *phase* of minimum ages for the older
317 earthquake occurs before the *phase* of maximum ages for the younger earthquake
318 (Figure 11a). OxCal provides graphical output (Figure 11b) of the modeled probability
319 density functions for each sample along with the likelihood distribution from the
320 radiocarbon measurement, and the probability density function of each earthquake age

321 and interval between earthquakes, which we summarise with the mean and 95.5%
322 probability range (Table 3).

323

324

325 **6. EARTHQUAKE AGES AND RECURRENCE**

326 The OxCal Bayesian model gives the age of the penultimate great earthquake as $870 \pm$
327 34 BP (2σ) with decreasing precision for each older earthquake (Figure 12a and Table
328 3)). This is a function of both the number of samples available, in part reflecting the
329 limits to coring depth, and the number of sites which record the earthquake. We do not
330 consider further the oldest three earthquakes (not shown in figure 12) as they are only
331 constrained by samples from one site (Copper River Delta) and the precision of the
332 estimated ages is poor, ± 180 to ± 300 years.

333

334 The mean recurrence interval for the seven earthquakes from EQ6, ~ 3550 cal yr BP, to
335 1964 is ~ 595 years. This average is heavily influenced by the relatively long interval,
336 883 ± 34 (2σ) years, between the EQ1 and 1964, compared to the intervals between the
337 older earthquakes (Figure 12b). The pre-1964 earthquakes have recurrence intervals
338 that range from ~ 420 to ~ 610 years, with a mean ~ 535 . While it would be preferable to
339 have more samples from more sites for EQ5 and EQ6 in order to better constrain their
340 ages and interval, it seems clear that the interval between the penultimate great
341 earthquake and 1964 is the longest recorded.

342

343 **7. DISCUSSION AND CONCLUSIONS**

344 Is the 1964 earthquake typical of other Late Holocene great earthquakes? In terms of
345 coastal stratigraphy we certainly see comparable sediments and biostratigraphy, but in
346 addition to the temporal variations discussed above, there are also spatial differences in
347 the paleoseismic record (Carver and Plafker, 2008; Hamilton and Shennan, 2005b;
348 Shennan and Hamilton, 2006). For example, the coseismic uplift recorded east of Cape
349 Yakataga correlates with the penultimate earthquake at numerous other sites (Figure
350 13), and may indicate a greater area of rupture than in 1964 (Shennan et al., 2009) yet
351 there is no evidence of coseismic subsidence at Kenai and Kasilof, on the Cook Inlet
352 shore of the Kenai Peninsula (Shennan and Hamilton, 2006) (Figure 1). The Kenai
353 record, along with archaeological evidence, led Hutchinson and Crowell (2007) to
354 suggest that the 1964 rupture zone comprises three segments that may not always
355 rupture together: Kodiak, Kenai and Prince William Sound.

356

357 It is critical to note that the longest and most comprehensive records all come from the
358 Prince William Sound segment and the area of flat slab subduction of the Yakutat
359 microplate (Figures 1 and 13) and at this stage we can draw three main conclusions
360 with respect to this region. First, multiple earthquake cycles over at least the past 4000
361 years in the Prince William Sound segment follow the same general pattern of co-
362 seismic uplift and subsidence as 1964 yet show net subsidence over this period at most
363 sites. To separate the effects of glacial isostatic adjustment, eustasy and interseismic
364 tectonic motions will require expansion of existing modeling approaches (Barlow et al.,
365 2012). Glacio-isostasy and eustasy produce differences in relative land and sea levels

366 that occur gradually through time and over distances on the order of 10s to 100s of
367 kilometers.

368

369 In contrast, we observe measurable differences in net motion over shorter distances, for
370 example, between Katalla and Puffy Slough, Katalla and Copper River Delta, described
371 above, and between the Suckling Hills/Cape Suckling and the marsh immediately to the
372 west, discussed by Shennan (2009). Therefore we consider the possibility of upper
373 plate faulting and slip on the megathrust contributing to these differences over short
374 distances, superimposed on the broader scale effects of glacio-isostasy (Barlow et al.,
375 2012; Shennan and Hamilton, 2010).

376

377 A schematic cross section of the plate boundary from Cook Inlet to the Malaspina
378 Glacier places the paleoseismic sites in a structural framework relative to the Aleutian
379 megathrust and either known or inferred upper plate faults (Figure 13). Accretion of the
380 upper crustal section of the Yakutat microplate begins at the Malaspina Glacier and
381 extends to the Ragged Mountain fault in the west. The upper plate is imbricated by
382 several faults with Holocene displacement. These include the Hanning and Patton Bay
383 faults at Montague Island which ruptured beneath Prince William Sound in 1964, the
384 Ragged Mountain fault at Katalla, the Cape Suckling – Bering Glacier fault, and several
385 faults located in the vicinity of Icy Bay and the Malaspina Glacier.

386

387 The pattern of regional surface displacement and upper crustal faulting during the 1964
388 earthquake provides some insight into viable hypotheses for contributing to net

389 Holocene uplift of at least 4 m at Katalla, and similar amounts indicated by mid-
390 Holocene marine molluscs at Bering Glacier (Shennan, 2009) and Cape Suckling
391 (Plafker and Rubin, 1967). Rupturing of the Prince William Sound segment of the
392 megathrust extended from beneath the southeastern edge of Cook Inlet to the Bering
393 Glacier region, whilst upper plate faulting propagated to the surface on the Hanning and
394 Patton Bay faults within Prince William Sound (Figure 13; Plafker, 1969). There was no
395 surface faulting at Cape Suckling, although a spike in uplift suggests reverse motion on
396 the Suckling Hills – Bering Glacier fault that was confined to the subsurface. There is no
397 evidence for surface faulting at Ragged Mountain in 1964.

398

399 We infer a local earthquake beneath Katalla that caused uplift ~500 cal yr BP and was
400 followed by interseismic subsidence prior to uplift of the coast in 1964. Does the former
401 event reflect blind reverse faulting beneath the Katalla Valley that is temporally
402 decoupled from great megathrust earthquakes? Certainly the structural setting of the
403 valley is amenable to the presence of a blind thrust given the complexly folded and
404 faulted rocks mapped at the surface (Winkler and Plafker, 1993) and evidence for
405 duplex thrust faulting where roof and floor thrusts cause doubling up of the crustal
406 section (Pavlis et al., 2012). Furthermore, modeling of GPS geodetic data shows that
407 the valley is part of a small tectonic block that is currently deforming and rotating
408 separately relative to the regions east of the Bering Glacier and west of Ragged
409 Mountain (Elliott, 2011).

410

411 We consider two hypotheses for faulting contributing to net Holocene uplift at Katalla,
412 the first focuses solely on the history of rupturing on the megathrust, the second invokes
413 uplift driven by a blind fault beneath the valley. We prefer the second hypothesis, but
414 cannot discount the first given the circumstantial nature of the paleoseismic and
415 geologic data.

416

417 Hypothesis 1: The megathrust beneath Katalla is subject to large earthquakes from time
418 to time that do not rupture the entire Prince William Sound segment. This is certainly
419 plausible given the expected heterogeneity of the megathrust interface near the western
420 edge of Yakutat microplate accretion. The ~500 cal yr BP uplift at Katalla may be such
421 an event, if so, it reversed the pattern of interseismic subsidence following the
422 penultimate great earthquake, that is, the great earthquake ~870 cal yr BP. If localized
423 uplift beneath the valley is repeated from time to time independent of great earthquakes
424 on the Prince William Sound segment then a modest amount of net uplift could
425 accumulate, contributing to the 4+ m over 7000 years. The primary problem with this
426 hypothesis is that we have found no evidence within cores for older events like that of
427 ~500 cal yr BP. All the other silt-peat couplets that indicate coseismic uplift at Katalla
428 correlate with similar horizons at Copper River Delta, Puffy Slough and the marshes
429 west of Cape Suckling over the last 2600 years. This implies a return period for
430 localized slip that is greater than 2100 years, a recurrence period that is of course,
431 common (Wesson et al., 2008) on upper plate faults that operate independent of the
432 megathrust for much of their history.

433

434 Hypothesis 2: There is a blind reverse fault beneath Katalla Valley, with a long
435 recurrence interval, which contributed to net uplift of 4+ m in the last 7000 years, even
436 though coseismic uplift in great megathrust earthquakes was followed by interseismic
437 subsidence. This hypothesis has the following merits: 1) the blind reverse fault model is
438 consistent with net uplift at Katalla but net subsidence at Copper River Delta and Puffy
439 Slough; 2) similar net uplift at Cape Suckling and Bering Glacier is explained by
440 activation of the Suckling Hills – Bering Glacier upper plate fault (Chapman et al., 2011),
441 with net subsidence in the marshes to the west, including Puffy Slough. 3) The blind
442 fault model is consistent with the complex structural geology (Bruhn et al., 2004; Pavlis
443 et al., 2012; Winkler and Plafker, 1993); T.L. Pavlis, personal communications, 2013)
444 surrounding and inferred to underlie the Katalla Valley.

445

446 Therefore our second conclusion is that contributions to net uplift may occur by both slip
447 on the megathrust and upper plate faulting (Figure 13), the latter leading to measurable
448 differences in coseismic uplift over a few kilometers.

449

450 Thirdly, the long interval between the penultimate and 1964 earthquake appears
451 unusual given the paleoseismic record for the last several thousand years. The reason
452 for this difference is uncertain given the available data. One possibility is that the long
453 return period simply reflects part of the natural variability in the time dependent behavior
454 of the megathrust. Another, is that the two events ~500 cal yr BP, one at Kodiak and
455 the other in the vicinity of Katalla, reduced the level of stress on the megathrust and
456 retarded rupturing across the whole area until 1964. The nature of the ~500 cal yr BP

457 events remains uncertain - slip on the megathrust is inferred by Carver and Plafker
458 (2008) at Kodiak, while imbricate faulting within the crust above the megathrust seems
459 more likely at Katalla. Whether it was it was a slipping patch on the megathrust or an
460 upper plate fault at Katalla, the Katalla and Kodiak events would have reduced stress in
461 those two regions, and possibly initiated creep, and hence time-dependent stress
462 release, on the megathrust beneath Prince William Sound, delaying the onset of seismic
463 rupturing until 1964?

464

465 One of the changes made in the 2007 modification to the seismic hazard maps for
466 Alaska was to change the assumed recurrence interval of great earthquakes in the
467 Prince William sound segment from 750 to 650 years, based upon the paleoseismic
468 research published at the time (Wesson et al., 2007). Although this made little change
469 to the hazard for most locations, enhancement of the paleoseismic records provides
470 better characterization of the megathrust and upper plate faults and therefore a more
471 satisfactory justification in terms of observation and understanding for calculating
472 seismic hazard. The age modeling results described above provide more reliable and
473 precise estimates of earthquake recurrence and could contribute to enhancements of
474 both time-dependent and time-independent seismic hazard analyses for Alaska. A
475 further enhancement would be to include the Katalla area as a source of seismic
476 hazard, similar to other locations in the western part of the Yakutat microplate, such as
477 the two M_w8+ ruptures in 1899 (Plafker and Thatcher, 2008).

478 **ACKNOWLEDGMENTS**

479 Sarah Cervera Heinlein, Peter Haeussler and Rich Koehler for help in the field;
480 Christopher Bronk Ramsey for guidance on Oxcal modeling; Gary Carver, George
481 Plafker and Terry Pavlis for discussions and comments concerning paleoseismology
482 and tectonics. This work is supported by the Saint Elias Erosion and Tectonics project
483 (STEEP), NSF 0408959, the U.S. Geological Survey, Department of the Interior,
484 earthquake hazards projects awards 06HQGR0033, G09AP00105 and G10AP00075
485 (The views and conclusions contained in this document are those of the authors and
486 should not be interpreted as necessarily representing the official policies, either
487 expressed or implied, of the U.S. Government) and NERC Radiocarbon Facility (grants
488 #935.0901 and #1339.1008). This work forms a contribution to IGCP Project 588
489 “Preparing for Coastal Change”.

490

491 **REFERENCES**

492

- 493 Atwater, B.F., Yamaguchi, D.K., Bondevik, S., Barnhardt, W.A., Amidon, L.J., Benson,
494 B.E., Skjerdal, G., Shulene, J.A., and Nanayama, F., 2001, Rapid resetting of an
495 estuarine recorder of the 1964 Alaska earthquake: Geological Society of America
496 Bulletin, v. 113, p. 1193-1204.
- 497 Barlow, N.L.M., Shennan, I., and Long, A.J., 2012, Relative sea-level response to Little
498 Ice Age ice mass change in south central Alaska: Reconciling model predictions
499 and geological evidence: Earth and Planetary Science Letters, v. 315-316, p. 62-
500 75.
- 501 Boyd, O.S., Zeng, Y., Bufe, C.G., Wesson, R.L., Pollitz, F., and Hardebeck, J.L., 2008,
502 Toward a time-dependent probabilistic seismic hazard analysis for Alaska, *in*
503 Freymueller, J.T., Haeussler, P.J., Wesson, R., and Ekström, G., eds., Active
504 Tectonics and Seismic Potential of Alaska, Volume 179: Geophysical Monograph
505 Series: Washington, DC, AGU, p. 399-416.
- 506 Bronk Ramsey, C., 2009, Bayesian analysis of radiocarbon dates: Radiocarbon, v. 51,
507 p. 337-360.
- 508 Bruhn, R.L., Pavlis, T.L., Plafker, G., and Serpa, L., 2004, Deformation during terrane
509 accretion in the Saint Elias orogen, Alaska: Geological Society of America
510 Bulletin, v. 116, p. 771-787.
- 511 Carver, G., and Plafker, G., 2008, Paleoseismicity and Neotectonics of the Aleutian
512 Subduction Zone - An Overview, *in* Freymueller, J.T., Haeussler, P.J., Wesson,
513 R., and Ekstrom, G., eds., Active tectonics and seismic potential of Alaska:
514 Geophysical Monograph Series: Washington, American Geophysical Union, p.
515 43-63.

516 Chapman, J.B., Worthington, L.L., Pavlis, T.L., Bruhn, R.L., and Gulick, S.P., 2011, The
517 Suckling Hills Fault, Kayak Island Zone, and accretion of the Yakutat microplate,
518 Alaska: *Tectonics*, v. 30, p. TC6011, doi:10.1029/2011TC002945.

519 Elliott, J., 2011, Active Tectonics in Southern Alaska and the role of the Yakutat Block
520 constrained by GPS measurements: Fairbanks, University of Alaska Fairbanks.

521 Hamilton, S., and Shennan, I., 2005, Late Holocene relative sea-level changes and the
522 earthquake deformation cycle around upper Cook Inlet, Alaska: *Quaternary*
523 *Science Reviews*, v. 24, p. 1479-1498.

524 Hamilton, S., Shennan, I., Combellick, R., Mulholland, J., and Noble, C., 2005, Evidence
525 for two great earthquakes at Anchorage, Alaska and implications for multiple
526 great earthquakes through the Holocene: *Quaternary Science Reviews*, v. 24, p.
527 2050-2068.

528 Hutchinson, I., and Crowell, A.L., 2007, Recurrence and Extent of Great Earthquakes in
529 Southern Alaska During the Late Holocene from an Analysis of the Radiocarbon
530 Record of Land-Level Change and Village Abandonment: *Radiocarbon*, v. 49, p.
531 1323-1385.

532 Knudson, B.M., 1954, The Ecology of the Diatom Genus *Tabellaria* in the English Lake
533 District: *Journal of Ecology*, v. 42, p. 345-358.

534 Lienkaemper, J.J., and Bronk Ramsey, C., 2009, OxCal: Versatile tool for developing
535 paleoearthquake chronologies - A primer: *Seismological Research Letters*, v. 80,
536 p. 431-434.

537 McCalpin, J., P, and Carver, G., 2009, Paleoseismology of compressional tectonic
538 environments, *in* McCalpin, J., P, ed., *Paleoseismology*, Volume 95: International
539 Geophysics Series: Burlington, Academic Press, p. 315 - 419.

540 Nelson, A.R., Shennan, I., and Long, A.J., 1996, Identifying coseismic subsidence in
541 tidal-wetland stratigraphic sequences at the Cascadia subduction zone of
542 western North America: *Journal of Geophysical Research*, v. 101, p. 6115-6135.

543 NOAA, 2013, <http://tidesandcurrents.noaa.gov/sltrends/index.shtml> Accessed August 1,
544 2013.

545 Patrick, R., and Reimer, C.W., 1966, The Diatoms of the United States. Volume 1.
546 Monographs of The Academy of Natural Sciences of Philadelphia No 13:
547 Philadelphia, Academy of Natural Sciences of Philadelphia, 688 p.

548 Pavlis, T.L., Chapman, J.B., Bruhn, R.L., Ridgway, K., Worthington, L.L., Gulick, S.P.S.,
549 and Spotila, J., 2012, Structure of the actively deforming fold-thrust belt of the St.
550 Elias orogen with implications for glacial exhumation and three-dimensional
551 tectonic processes: *Geosphere*, v. 8, p. 991-1019.

552 Plafker, G., 1969, Tectonics of the March 27, 1964, Alaska earthquake: U.S. Geological
553 Survey Professional Paper, v. 543-I, p. 74.

554 —, 1987, Regional geology and petroleum potential of the northern Gulf of Alaska
555 continental margin, *in* Scholl, D.W., Grantz, A., and Vedder, J.G., eds., *Geology*
556 *and Resource Potential of the Continental Margin of Western North America and*
557 *Adjacent Ocean Basins - Beaufort Sea to Baja California*, Volume 6: Earth
558 Science Series: Houston, Circum-Pacific Council for Energy and Mineral
559 Resources, p. 229-268.

560 Plafker, G., Lajoie, K.R., and Rubin, M., 1992, Determining intervals of great subduction
561 zone earthquakes in southern Alaska by radiocarbon dating, *in* Taylor, R.E.,

562 Long, A., and Kra, R.S., eds., Radiocarbon after four decades. An
563 interdisciplinary perspective: New York, Springer Verlag, p. 436-452.

564 Plafker, G., and Rubin, M., 1967, Vertical tectonic displacements in south central Alaska
565 during and prior to the great 1964 earthquake: *Journal of Geoscience*, v. 10, p. 1-
566 7.

567 Plafker, G., and Thatcher, W., 2008, Geological and geophysical evaluation of the
568 mechanisms of the Great 1899 Yakutat Bay Earthquakes, *in* Freymueller, J.T.,
569 Haeussler, P.J., Wesson, R., and Ekström, G., eds., *Active Tectonics and*
570 *Seismic Potential of Alaska*, Volume 179: Geophysical Monograph Series:
571 Washington, DC, AGU, p. 215-236.

572 Richards, S.W., 2000, Holocene history of the Katalla River Valley, Alaska: Salt Lake
573 City, Univeristy of Utah.

574 Shennan, I., 2009, Late Quaternary sea-level changes and palaeoseismology of the
575 Bering Glacier region, Alaska: *Quaternary Science Reviews*, v. 28, p. 1762-1773.

576 Shennan, I., Bruhn, R., and Plafker, G., 2009, Multi-segment earthquakes and tsunami
577 potential of the Aleutian megathrust: *Quaternary Science Reviews*, v. 28, p. 7-13.

578 Shennan, I., and Hamilton, S., 2006, Coseismic and pre-seismic subsidence associated
579 with great earthquakes in Alaska: *Quaternary Science Reviews*, v. 25, p. 1-8.

580 Shennan, I., and Hamilton, S.L., 2010, Holocene sea-level changes and earthquakes
581 around Bering Glacier, *in* Shuchman, R., Josberger, E., and Jenkins, L., eds.,
582 *Bering Glacier: Interdisciplinary studies of Earth's largest temperate surging*
583 *glacier: Geological Society of America Special Paper 462: Boulder, Geological*
584 *Society of America*, p. 275 - 290

585 Sirkin, L., and Tuthill, S.J., 1971, Late Pleistocene palynology and stratigraphy of
586 Controller Bay region, Alaska, *in* Ters, M., ed., *Études sur le quaternaire dans le*
587 *monde : VIIIe Congrès INQUA, Paris, 1969, Volume 1: Paris, Centre National de*
588 *la Recherche Scientifique*, p. 197-208.

589 Tysdal, R.G., Hudson, T., and Plafker, G., 1976, Surface features and recent movement
590 along the Ragged Mountain fault, south-central Alaska, U.S. Geological Survey
591 *Miscellaneous Field Studies Map MF-782*, 1 sheet, scale 1:24000.

592 Watcham, E.P., Shennan, I., and Barlow, N.L.M., 2013, Scale considerations in using
593 diatoms as indicators of sea-level change: lessons from Alaska: *Journal of*
594 *Quaternary Science*, v. 28, p. 165-179.

595 Wesson, R.L., Boyd, O.S., Mueller, C.S., Bufe, C.G., Frankel, A.D., and Petersen,
596 M.D., 2007, Revision of time-independent probabilistic seismic hazard
597 maps for Alaska, U.S. Geological Survey Open-File Report, Volume 2007-1043,
598 p. 1-33.

599 Wesson, R.L., Boyd, O.S., Mueller, C.S., and Frankel, A.D., 2008, Challenges in making
600 a seismic hazard map for Alaska and the Aleutians, *in* Freymueller, J.T.,
601 Haeussler, P.J., Wesson, R., and Ekström, G., eds., *Active Tectonics and*
602 *Seismic Potential of Alaska*, Volume 179: Geophysical Monograph Series:
603 Washington, DC, AGU, p. 385-397.

604 Winkler, G.R., and Plafker, G., 1993, Geologic map of the Cordova and Middleton
605 Island quadrangles, Southern Alaska, U.S. Geological Survey *Miscellaneous*
606 *Investigations Series Map 1984*, 1 sheet, scale 1:250,000., U.S. Geological
607 Survey.

608
609

610 **FIGURE CAPTIONS**

611 Figure 1: Tectonic setting of south central Alaska. Approximate area of coseismic
612 subsidence (light grey) and uplift (dark grey) in 1964 and the western segment of the
613 Yakutat microplate (dotted). Extent of subducted Yakutat slab shown to 50 km depth.
614 Star symbols indicate epicentre of two M_w8+ earthquakes in 1899. Note that
615 Hutchinson and Crowell (2007) adopt a further subdivision, with the Prince William
616 Sound segment partitioned into two, distinguishing a Kenai segment, the part beneath
617 the Kenai Peninsula not underlain by the subducted Yakutat slab.

618

619 Figure 2: LANDSAT image, 2013, of the coastal setting of the new field sites.

620

621 Figure 3: Copper River Delta: exposure of two silt-peat couplets at location 3 discussed
622 in the text; coring revealed a third couplet.

623

624 Figure 4: Copper River Delta - Alaganik Slough sampling locations; a) 2013 LANDSAT
625 image; b) air photo, August 1952; c) summary stratigraphy at sample locations, black =
626 peat, adjacent triangle = sharp contact, white = silt, tree root symbol where present,
627 calibrated age 95% age ranges BP (details in table 2); d) summary diatom diagram
628 showing species accounting for >10% in at least one sample, and summary salinity
629 classes, depths in cm relative to silt-peat contact.

630

631 Figure 5: Copper River Delta, mean and 95% uncertainty model estimates of paleo
632 marsh surface elevation change across silt-peat couplets using the diatom-based
633 transfer function method described in the text.

634

635 Figure 6: a) LANDSAT image of Katalla River Valley and Puffy Slough, with marshes
636 numbered and individual sample locations indicated by white circles ; b) air photo
637 mosaic of the area, August 1950. Note the extent of tidal inundation and difference in
638 vegetation extent, c) Katalla River summary stratigraphy and geomorphology along

639 transect X' - X, black = peat, white = silt, stipple = sand (top contacts of all silt and sand
640 units shown are sharp) and calibrated age 95% age ranges cal yr BP (details in table 2);
641 d) Puffy Slough, example of a core recording four episodes of coseismic uplift (the base
642 of the surface peat represents uplift in 1964) superimposed upon net submergence.

643

644 Figure 7: Katalla site 3.10 summary diatom diagram and reconstruction estimates of
645 paleo surface marsh elevations with 95% confidence limits: showing species accounting
646 for >10% in at least one sample, total count per sample, radiocarbon ages cal yr BP and
647 summary salinity classes, depths in cm relative to present ground surface; for elevation
648 reconstructions, diamond symbol indicates low count, 125 diatoms, all others shown are
649 based on >200. Grey symbol fill indicates close modern analogue, white indicates poor
650 modern analogue.

651

652 Figure 8: Katalla site 5.5 summary diatom diagram and photograph of box sample
653 across the contact, showing species accounting for >10% in at least one sample, total
654 count per sample, and summary salinity classes, depths in cm relative to present
655 ground surface.

656

657 Figure 9: a) marsh stratigraphy exposed along Katalla River, at site 5.5; b) 25 cm box
658 section sampled across the contact at site 5.5; c) box sample across silt-peat contact,
659 showing sand layer within the silt unit, sample taken near to Copper River Delta site 3.

660

661 Figure 10: Comparison of radiocarbon ages on paired samples of bulk peat and
662 herbaceous macrofossils.

663

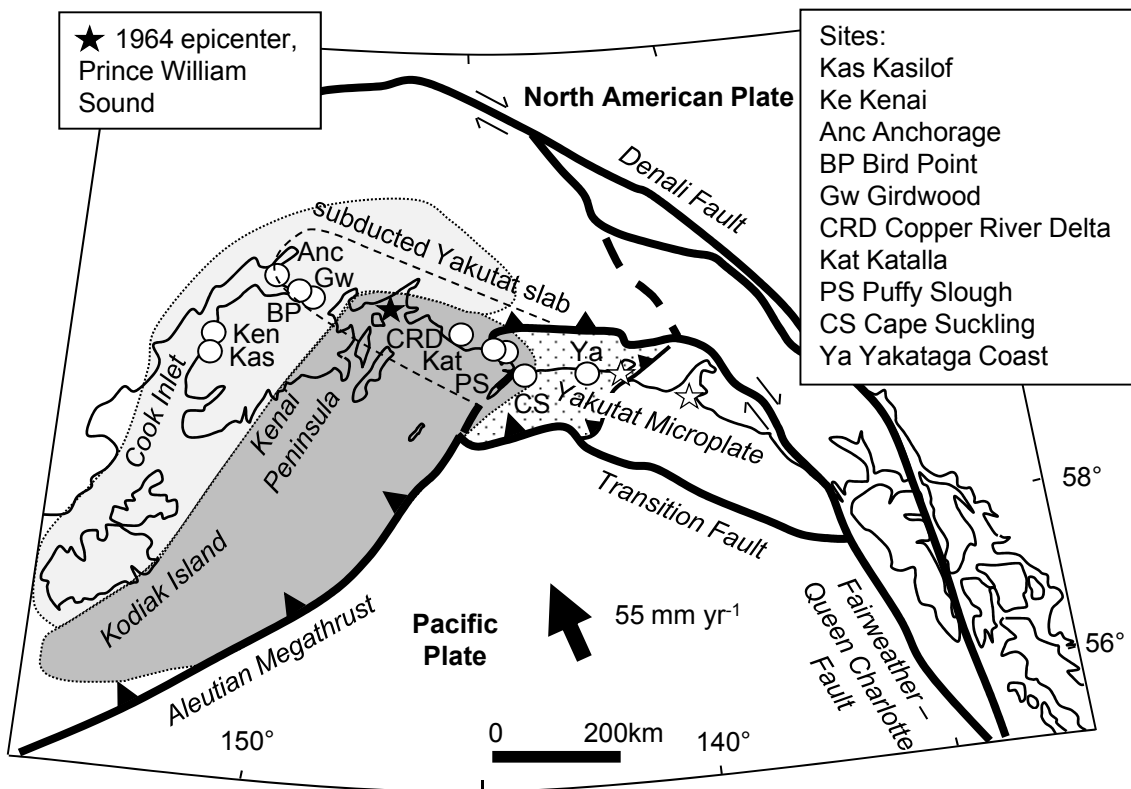
664 Figure 11: Age model of earthquake recurrence, a – Oxcal model structure of phases for
665 constraining earthquake ages (Lienkaemper and Bronk Ramsey (2009) ; b – example of
666 model input and output, for just EQ 1. The full model repeats this for each earthquake.
667 Input:for each sample within a phase the calibrated age, in grey. Outputs in black, the
668 probability density function from Bayesian modelling for each input sample and the
669 95.4% probability age of the intervening earthquake.

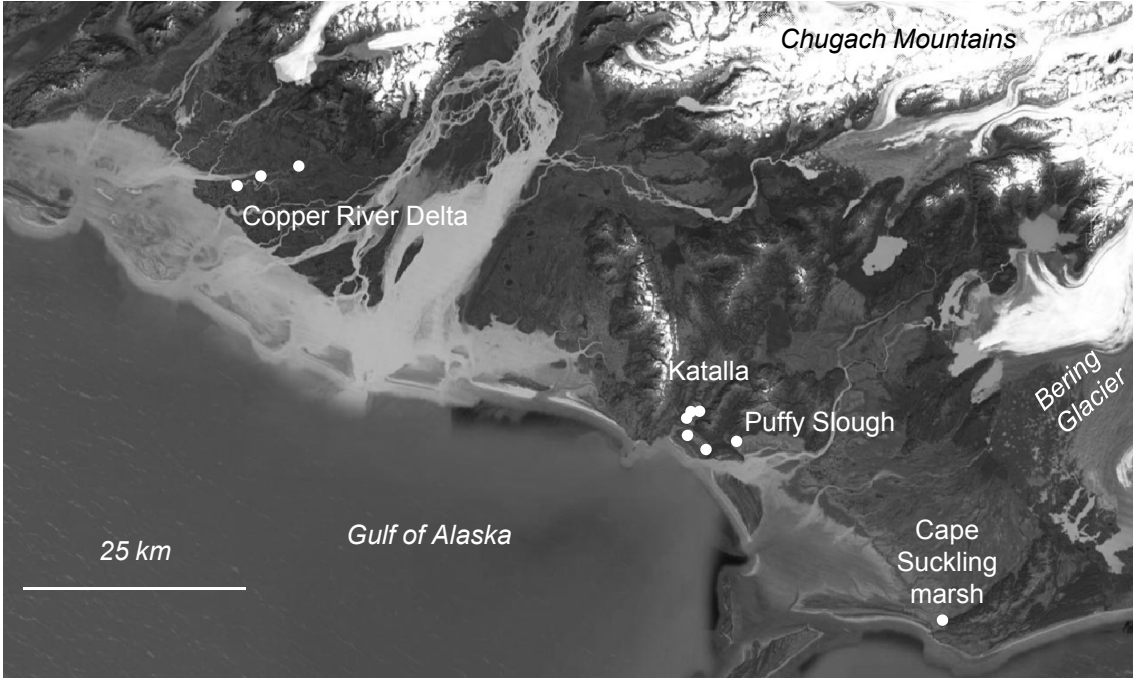
670

671 Figure 12: Probability density functions for earthquake ages (a) and intervals (b).

672

673 Figure 13: .Schematic cross section of the plate boundary from Cook Inlet to the
674 Malaspina Glacier, with summary of major earthquakes, direction of coseismic
675 deformation and net Holocene motion: grey = no data of that age, \uparrow uplift, \downarrow
676 subsidence, \square no deformation. Large crustal faults are either known from surface
677 offsets or inferred from paleoseismology and/or geologic mapping. The Ragged
678 Mountain fault is a thrust fault that sutures the Yakutat terrane to the Early Tertiary
679 Alaskan plate margin. That fault is marked by a 30 km-long system of Quaternary
680 normal fault scarps that may reflect reactivation in extension (Tysdal et al., 1976), or
681 possibly flexure above the tip of a buried thrust fault. The faults between Ragged
682 Mountain and the Suckling Hills are inferred blind thrust faults within a complicated
683 stack of imbricate thrusts that form an anticline beneath the Katalla Valley, but may have
684 little or no surface manifestation other than uplift in the valley. The faults are inferred
685 from geologic mapping (T.L. Pavlis, personal communications, 2013) and local uplift in
686 the valley ~500 cal yr BP as discussed in section 7. The Suckling Hills and Bering
687 Glacier faults are part of the same fault system that link to the Kayak Island Zone
688 offshore (Chapman et al., 2011). The fault beneath Icy Bay is the Malaspina thrust fault
689 which is known from both drill hole data (Chapman et al., 2011; Plafker, 1987) and
690 geodetic observations (e.g. (Elliott, 2011)).



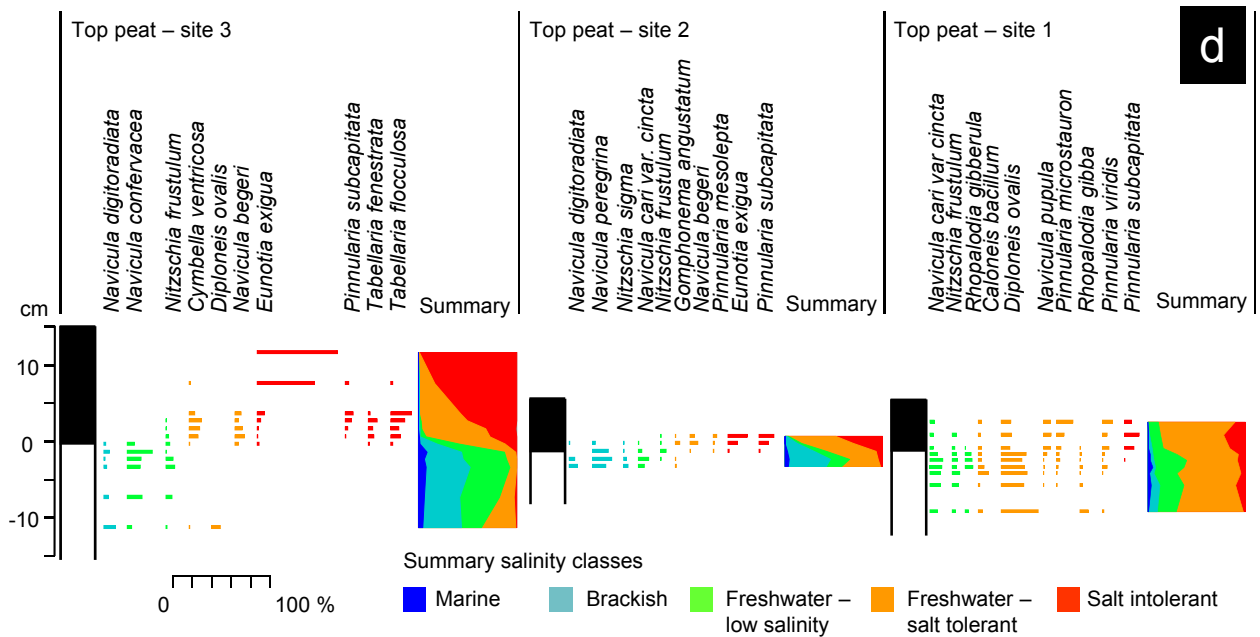
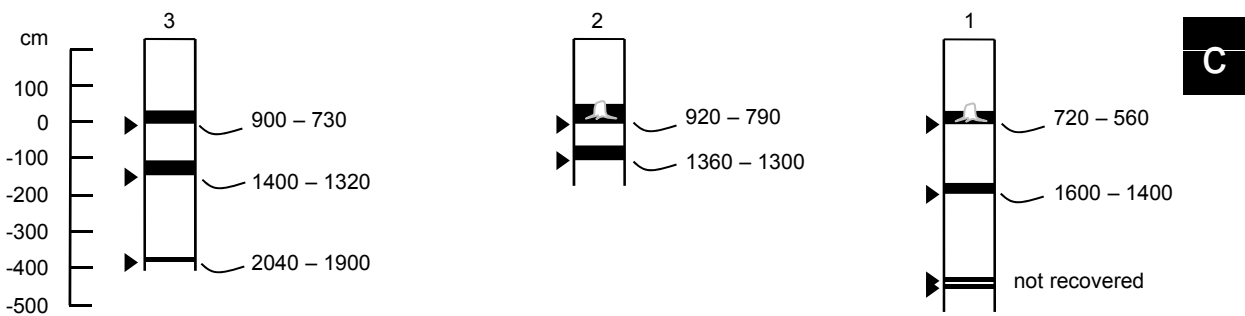
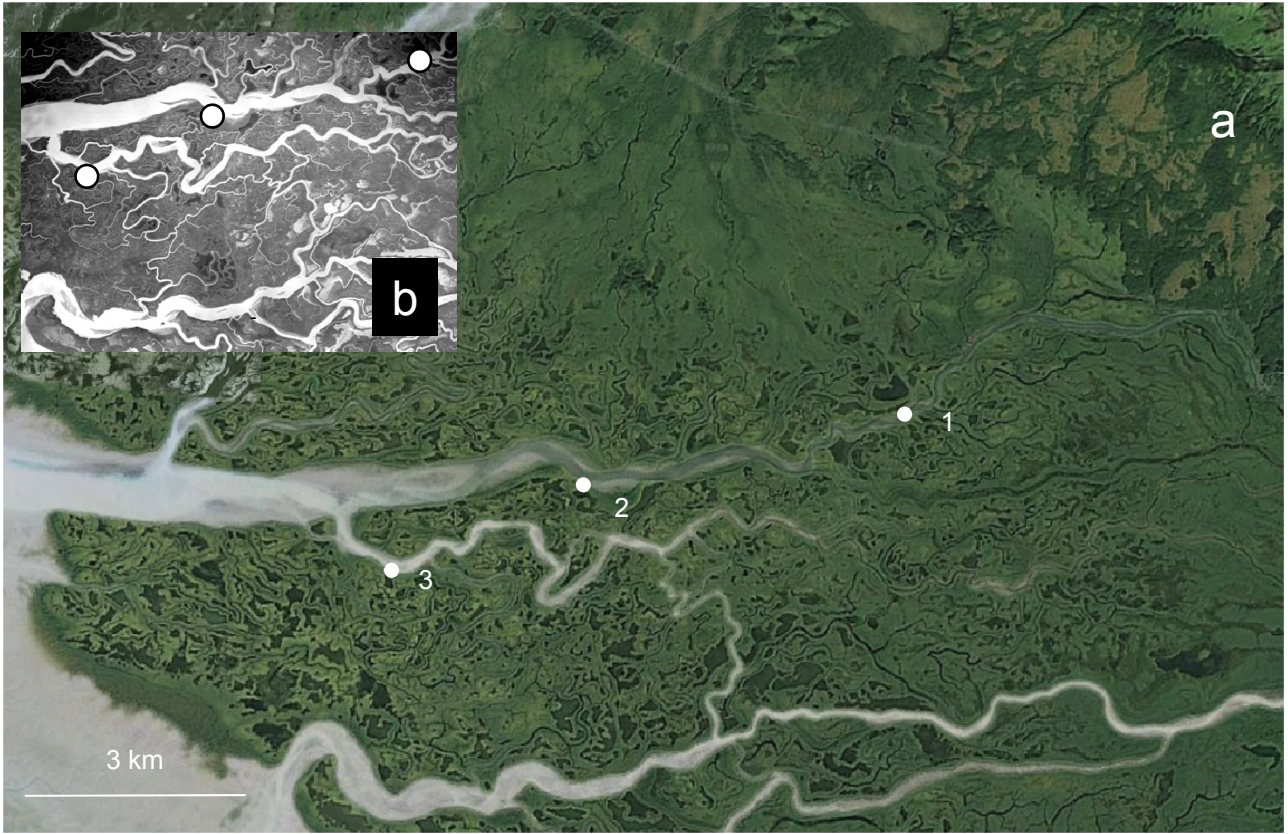


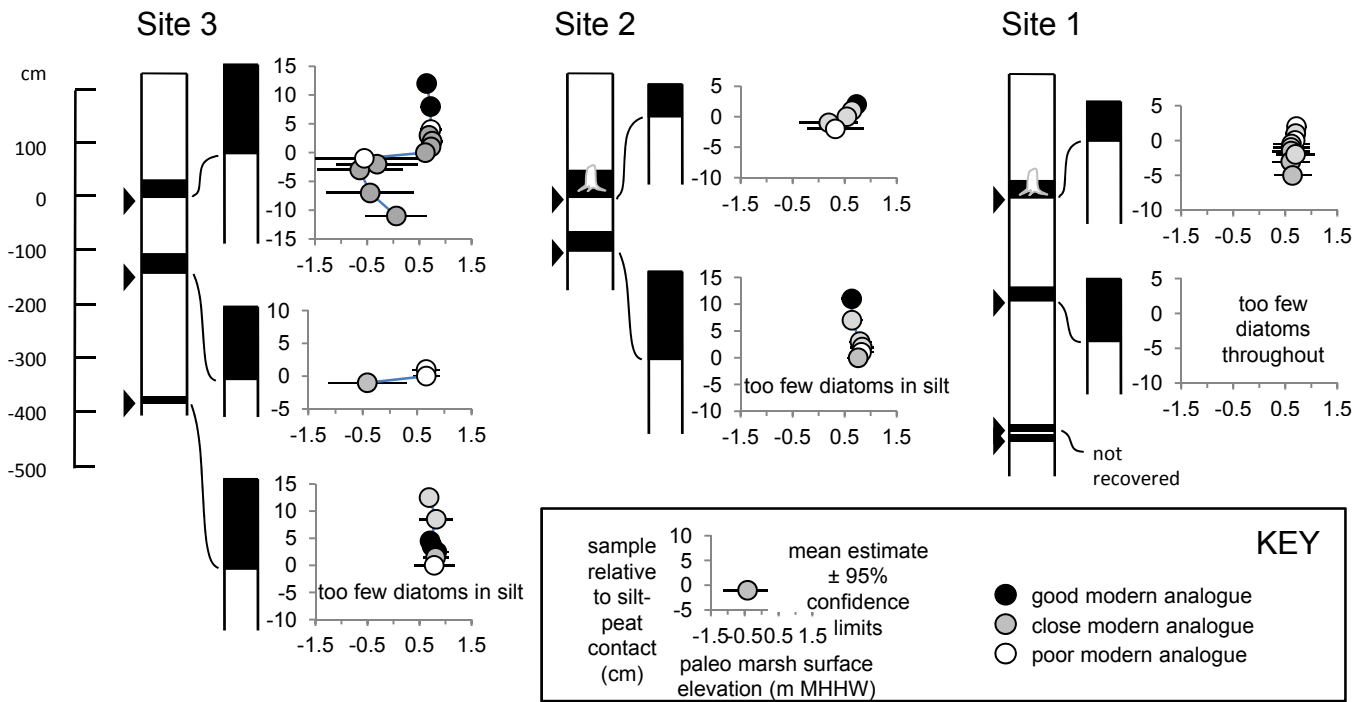


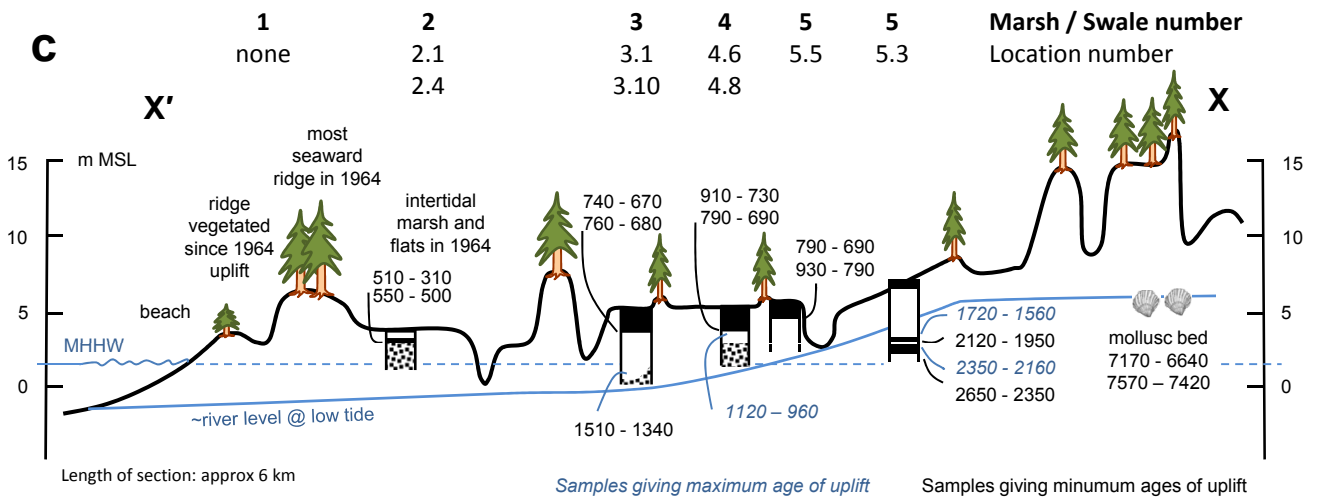
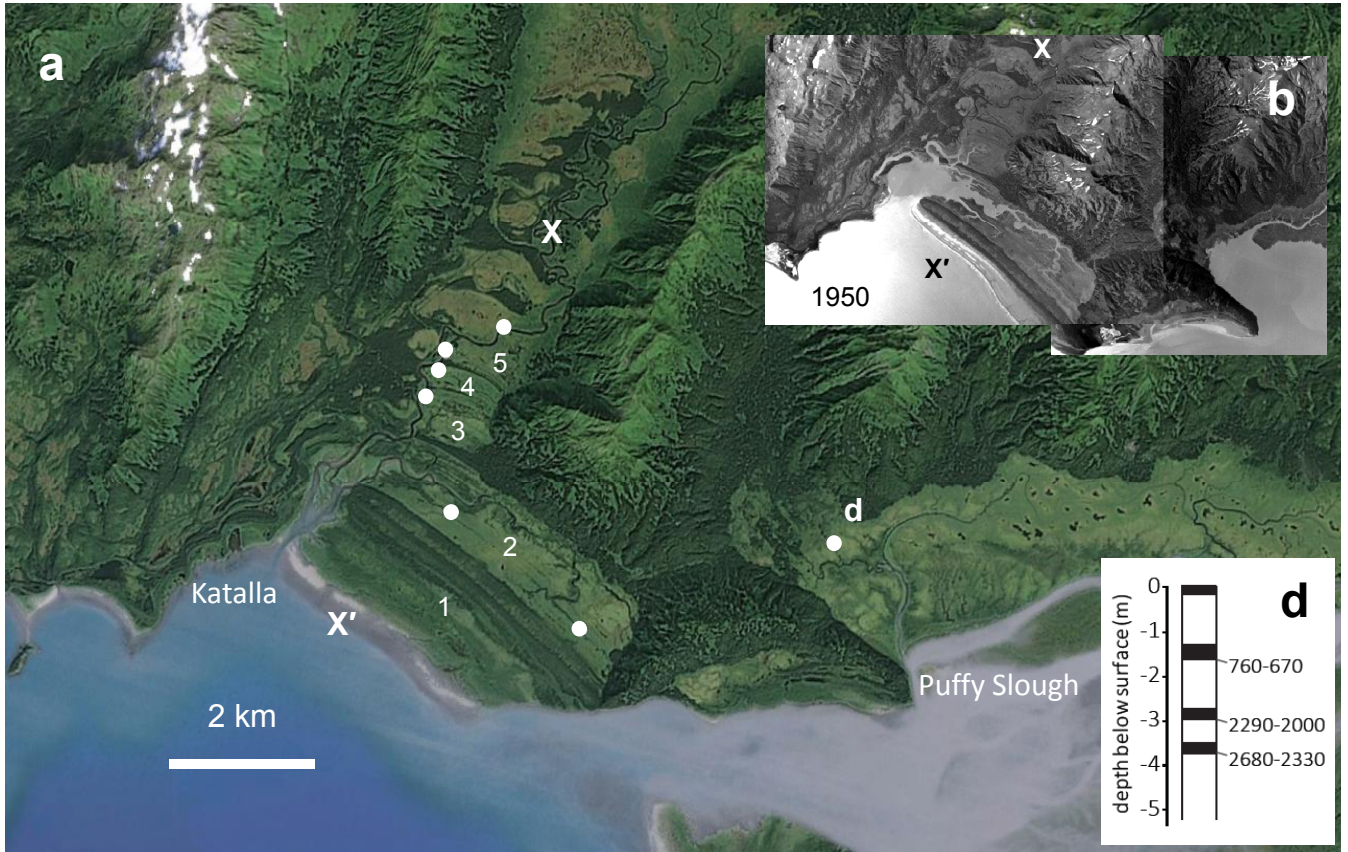
Depth below
surface of
modern high
marsh
~0.50 m

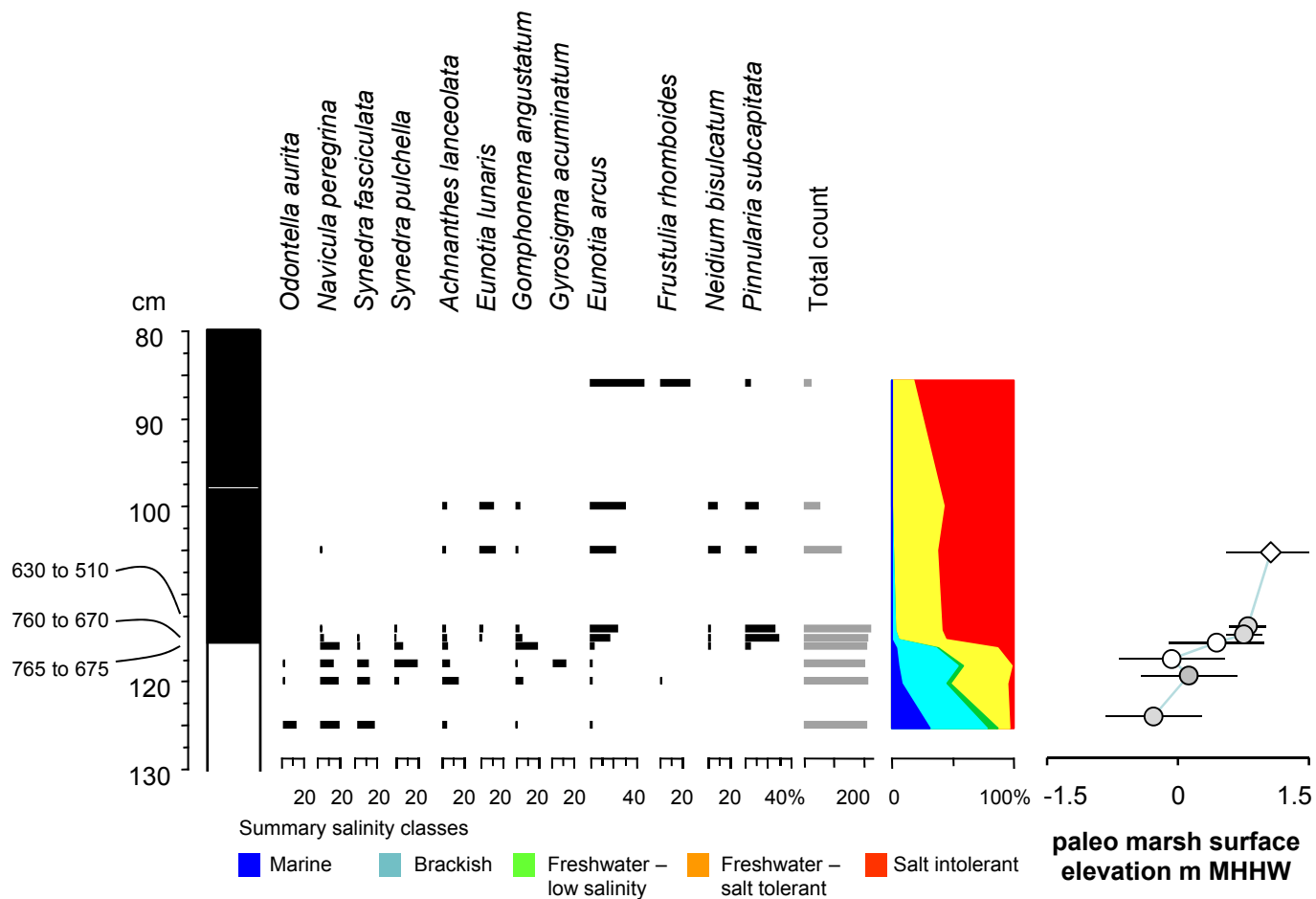
~1.25 m

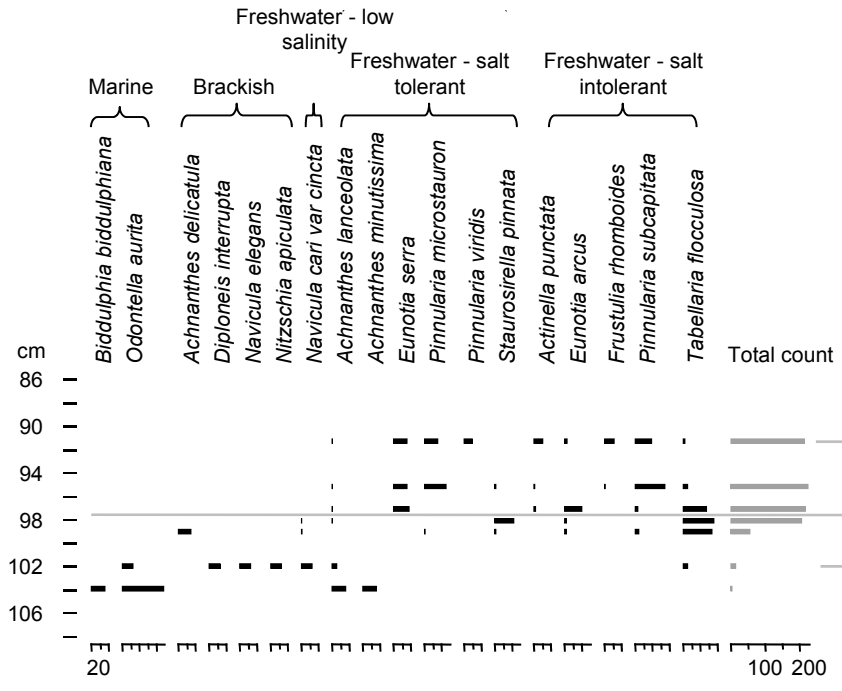
~2.70 m





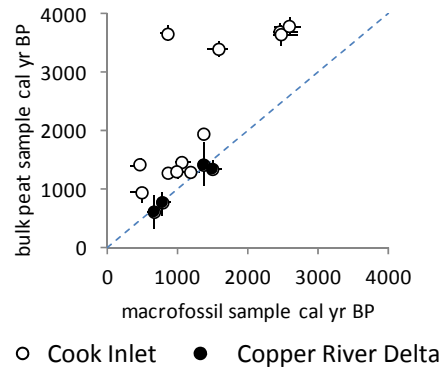




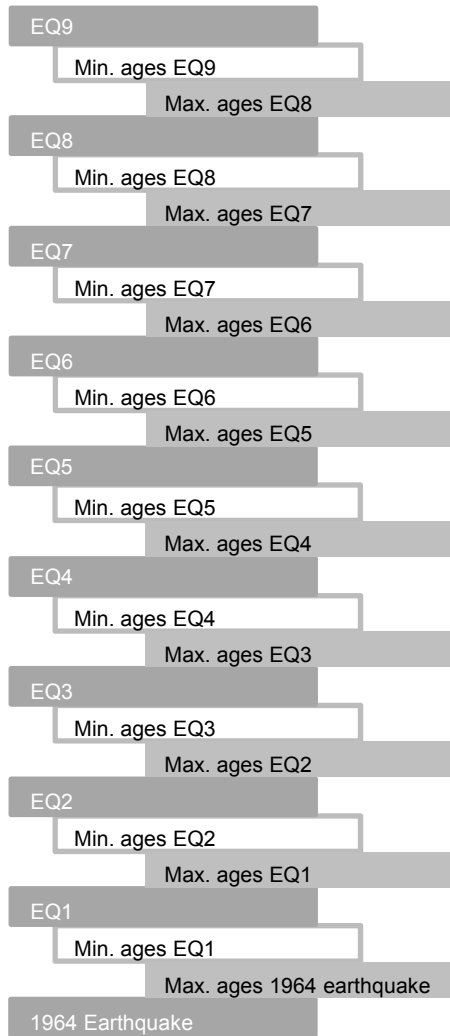




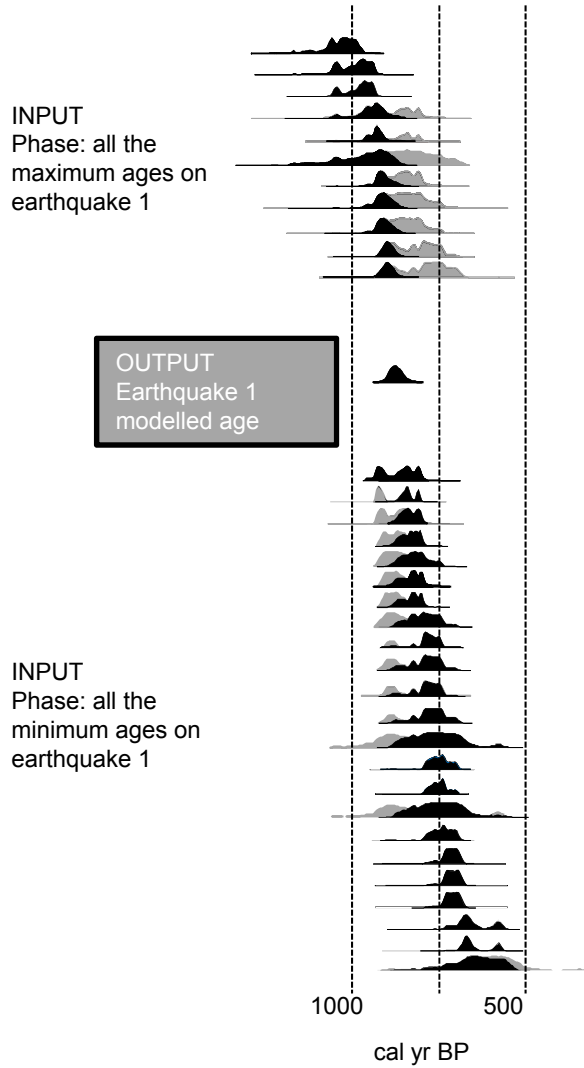
Radiocarbon age comparisons

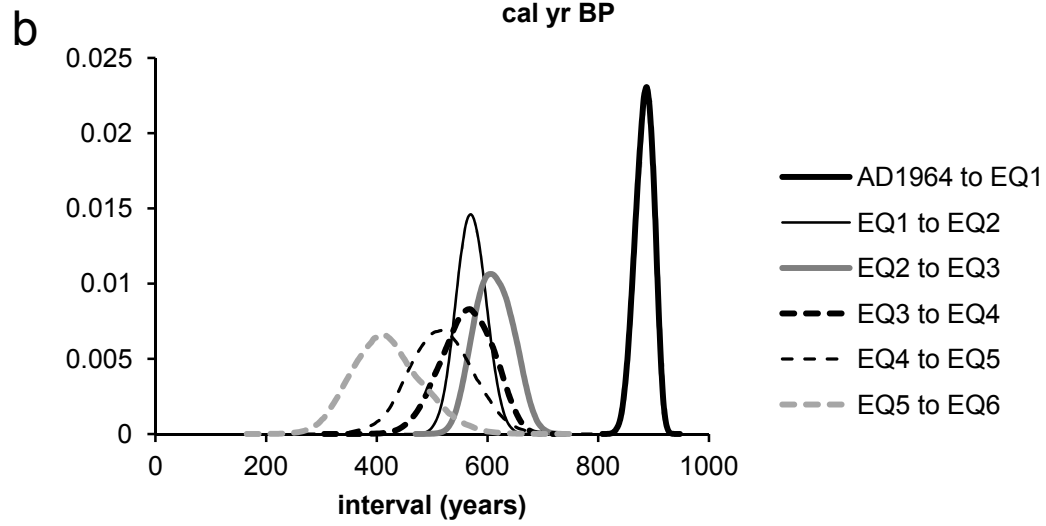
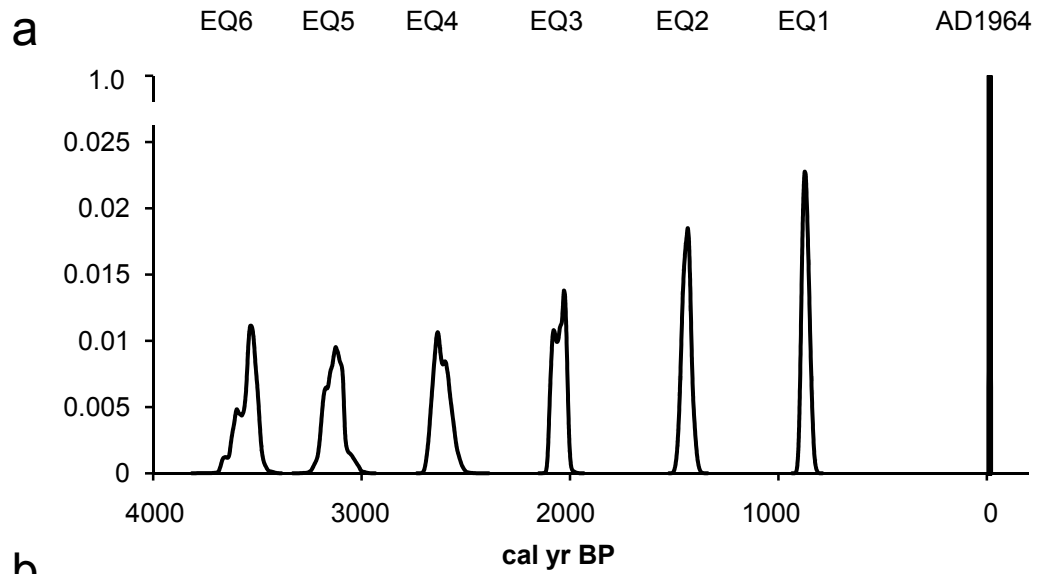


a) Full model structure



b) Example model output: EQ1





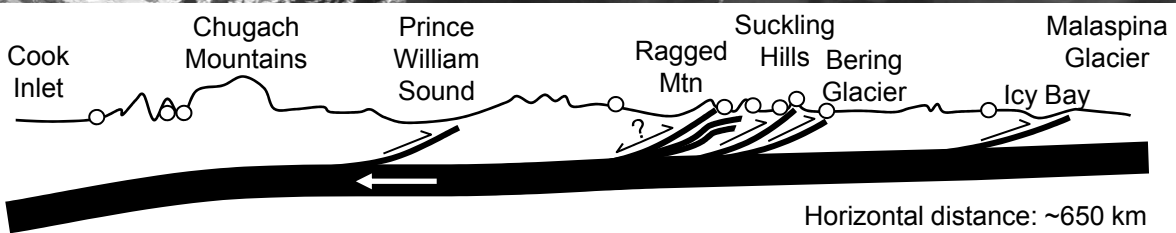
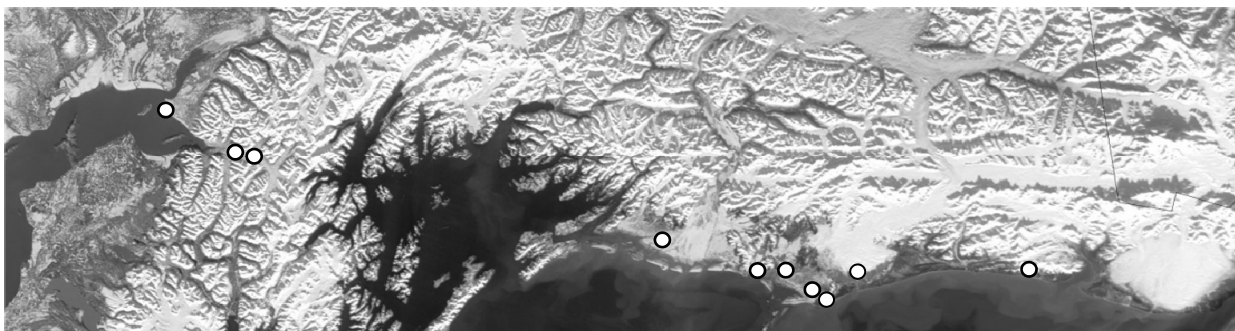
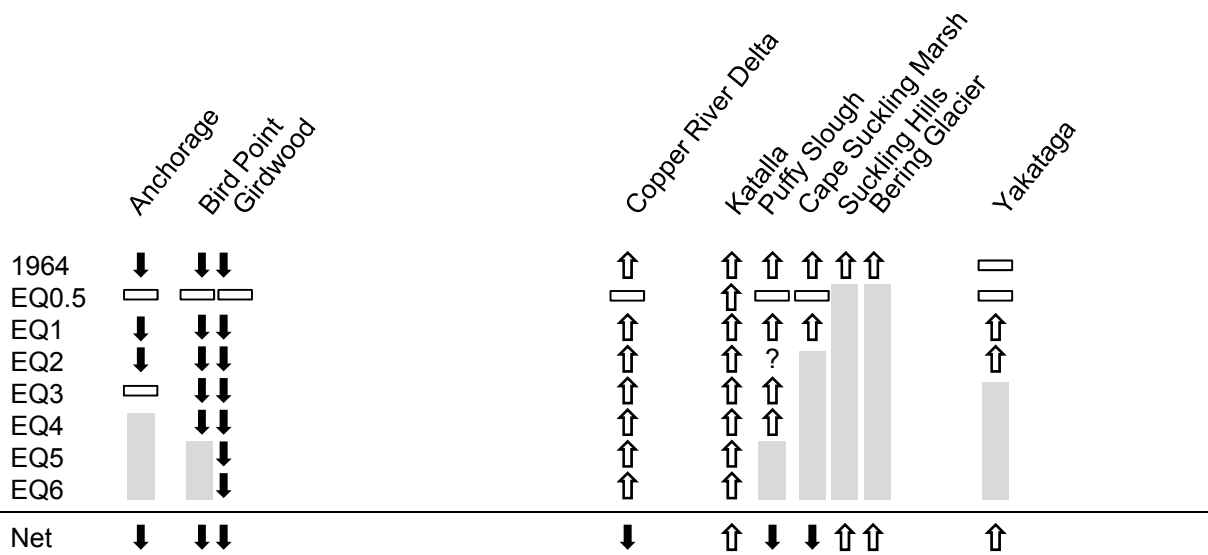


Table 1: Summary statistics for transfer function models used to reconstruct paleo marsh surface elevations. All models use modern samples from the regional-scale dataset covering sites across south-central Alaska (Full details of modern samples and model development in Hamilton and Shennan (2005) and Watcham et al., (2013)).

	Model 1	Model 2	Model 3
Number of samples in modern training set	100	206	255
Number of components in weighted averaging partial least squares model ¹	2	2	2
Squared correlation between bootstrap predicted and observed values (r^2)	0.75	0.68	0.76
Root mean squared error of prediction (bootstrap RMSEP)	6.31	11.94	17.48
Improvement in RMSEP over one-component model	14.7%	11.4%	10.5%
RMSEP scaled to tidal range at Katalla and Copper River Delta	0.10 m	0.19 m	0.27 m
Model applicable to lithology of fossil sample	Peat	Silt with herbaceous rootlets ²	Silt , no visible rootlets

¹ We assessed model performance using r^2 , scatterplots of observed and predicted values, and RMSEP, with the best models being those with the highest r^2 value, a linear distribution of observed plotted against predicted values, and the lowest RMSEP, but only if the RMSEP was improved by at least 5% with the addition of an extra component.

² Where there was no good or close modern analogue using model 2 for a silt unit with herbaceous rootlets we would apply model 3 if it gave at least a close modern analogue, indicating a better fit but with a larger uncertainty term.

Table 2: New Radiocarbon dates

All samples on herbaceous macrofossil stem/leaves picked from peat or silt matrix

Lab code	Site	Sample	Description	depth below core or section datum	core or section datum m MHHW	14C BP	SD	Range (cal yr BP)	
Copper River Delta: Alaganik Slough									
Beta-223760	AS 1	AS/06/1/2	Base of peat 1	110	~1	700	40	559	to 721
Beta-223761	AS 1	AS/06/1/3	Base of peat 2	310	~1	1610	40	1403	to 1601
Beta-266415	AS 3	AS/09/3/1	Base of peat 1	75	~1	880	20	733	to 901
Beta-266416	AS 3	AS/09/3/2	Base of peat 2	145	~1	1480	20	1318	to 1402
Beta-266417	AS 2	AS/09/4	Base of peat 1	75	~1	930	20	793	to 915
Beta-266418	AS 3	AS/09/5	Base of peat 3	436	~1	2020	20	1900	to 2037
Beta-266419	AS 2	AS/09/8	Base of peat 2	175	~1	1430	20	1296	to 1356
Katalla									
Beta - 318153	Ka 2.1	KR/07/1B/40	5cm above base of peat	40	~2.4	240	30	-1	to 424
Beta - 318154	Ka 2.1	KR/07/1B/42	3cm above base of peat	42	~2.4	270	30	0	to 435
Beta - 239237	Ka 2.1	KA/07/1A/45	Base of peat layer	45	~2.4	400	40	318	to 518
Beta - 239238	Ka 2.4	KA/07/4/71	Base of peat layer	71	~2.4	530	40	506	to 638
Beta - 316245	Ka 3.1	KR11-1-381	Within silt layer, above sand	381	~3.9	1510	30	1319	to 1515
Beta - 316246	Ka 5.3	KR11-3-35	Top of peat layer	35	~2	1740	30	1562	to 1715
Beta - 316247	Ka 5.3	KR11-3-50	1cm above base of peat layer	50	~2	2030	30	1898	to 2105
Beta - 316248	Ka 5.3	KR11-3-51	Base of peat layer	51	~2	2060	30	1948	to 2118
Beta - 316249	Ka 5.3	KR11-3-62	Top of peat layer	62	~2	2270	30	2158	to 2347
Beta - 316250	Ka 5.3	KR11-3-81	Base of peat layer	81	~2	2390	30	2344	to 2675
Beta - 316251	Ka 5.5	KR11-5-27	Base of peat layer above freshwater silt unit	27	~4.2	110	30	-4	to 269
Beta - 316252	Ka 5.5	KR11-5-96	1cm above base of peat layer	96	~4.2	830	30	686	to 789
Beta - 316253	Ka 5.5	KR11-5-97	Base of peat layer	97	~4.2	950	30	794	to 926
Beta - 316254	Ka 4.6	KR11-6-122	2cm above base of peat layer	122	~3.9	880	30	729	to 907
Beta - 316255	Ka 4.6	KR11-6-124	Base of peat layer	124	~3.9	840	30	685	to 892
Beta - 316256	Ka 4.6	KR11-6-127	Within silt layer, below peat contact	127	~3.9	1130	30	962	to 1167
Beta - 316257	Ka 4.8	KR11-8-190	Within silt layer, above sand	190	~3.9	1250	30	1082	to 1273
Beta - 316258	Ka 3.10	KR11-10-111	4cm above base of peat layer	111	~3.9	530	30	510	to 629
Beta - 316259	Ka 3.10	KR11-10-113	2cm above base of peat layer	113	~3.9	790	30	671	to 761
Beta - 316260	Ka 3.10	KR11-10-115	Base of peat layer	115	~3.9	800	30	675	to 765
Puffy Slough									
Beta - 328272	PF 4	PF/07/4 - 374	Base of lowest peat	374	~2	2370	40	2331	to 2682
Beta - 328271	PF 4	PF/07/4 - 370	Above base of lowest peat	370	~2	2170	30	2065	to 2311
Beta - 328270	PF 4	PF/07/4 - 260	Base of middle peat	260	~2	2120	30	1999	to 2293
Beta - 328269	PF 4	PF/07/4 - 258	2 cm above base of middle peat	258	~2	1320	30	1179	to 1298
Beta - 328268	PF 4	PF/07/4 - 153	Base of upper peat	153	~2	790	30	671	to 761
Beta - 328267	PF 4	PF/07/4 - 152	1cm above base of upper peat	152	~2	390	30	320	to 509

Table 3: Age model summary of earthquake ages and intervals. Oxcal model outputs for individual probability density functions, showing range (95.4% probability), mean, standard deviation, and median; and number of sites and number of samples recording each earthquake in model input. Older earthquakes not shown as they are less well constrained due to small sample sizes and are recorded at a single site.

Modelled age (years BP)	from	to	%	μ	σ	m	n_{sites}	n_{samples}
EQ1	902	837	95.4	870	17	871	9	34
EQ2	1484	1397	95.4	1440	21	1441	7	17
EQ3	2102	2006	95.4	2052	27	2050	6	9
EQ4	2685	2540	95.4	2615	38	2618	5	13
EQ5	3216	3037	95.4	3131	43	3131	2	5
EQ6	3662	3475	95.4	3550	47	3541	1	7
Modelled interval (years)								
AD1964 to EQ1	850	915	95.4	883	17	885		
EQ1 to EQ2	517	625	95.4	571	27	571		
EQ2 to EQ3	545	680	95.4	611	35	611		
EQ3 to EQ4	470	653	95.4	563	47	565		
EQ4 to EQ5	403	635	95.4	517	58	516		
EQ5 to EQ6	299	550	95.4	419	64	415		
Mean interval AD1964 to EQ6	518	558	95.4	536	10	535		
Mean interval EQ1 to EQ6	579	612	95.4	594	8	593		

Shennan et al: supplementray information table
 Radioacarbon data and age model structure for Oxcal age modelling

Site Codes

Kas Kasilof; Ke Kenai; Anc Anchorage; BP Bird Point; Gw Girdwood; CRD Copper River Delta; Kat Katalla; PS Puffy Slough; CS Cape Suckling; Ya Yakataga Coast

Literature sources

New: this paper table 2

1: Carver & Plafker 2008

2: Shennan et al. 2008

3: Barlow et al., 2012

4: Hamilton & Shennan, 2005

5: Shennan & Hamilton, 2006

6: Hamilton et al., 2005

7: Shennan 2009

8: Shennan et al., 2009

Lab code	14C BP	SD	Site	Sample code	Source	Description	Boundary	Constraint
							Earthquake 9	
W-6356	4860	90	CRD	91APR604N2	1	Alaganic Slough 0.5km below boat ramp		Minimum
W6360	4650	100	CRD	91APR606Y	1	Upper Alaganic Slough redrill		Minimum
							Earthquake 8	
CAMS-16583	4340	90	CRD	93APR25R	1	Alaganic Slough 0.1km above boat ramp		Minimum
CAMS-16573	4210	60	CRD	93APR21SS	1	Alaganic Slough 0.5km below boat ramp		Minimum
W-6355	4180	80	CRD	91APR604L	1	Alaganic Slough 0.5km below boat ramp		Minimum
CAMS-16579	3810	70	CRD	93APR23W	1	Alaganic Slough 1.4km above boat ramp		Minimum
							Earthquake 7	
W-6353	3690	50	CRD	91APR604I	1	Alaganic Slough 0.5km below boat ramp		Minimum
CAMS-16581	3680	60	CRD	93APR25N	1	Alaganic Slough 0.1km above boat ramp		Minimum
CAMS-16578	3640	90	CRD	93APR23T	1	Alaganic Slough 1.4km above boat ramp		Minimum
W6358	3600	90	CRD	91APR606R	1	Upper Alaganic Slough redrill		Minimum
							Phase boundary	
Beta-223764	3490	40	Gw	GW5/1	2	Upper boundary of Girdwood peat Y		Maximum
CAMS-16577	3280	60	CRD	93APR23M	1	Alaganic Slough 1.4km above boat ramp		Maximum

AA5640	3202	57	CRD	89APR502X	1	100 m upstream of boat ramp	Maximum
Earthquake 6							
W6549	3420	60	CRD	93APR25G	1	Alaganic Slough 0.1km above boat ramp	Minimum
AA5764	3279	102	CRD	89APR503M	1	Upper Alaganic Slough	Minimum
CAMS-16572	3180	60	CRD	93APR21FF	1	Alaganic Slough 0.5km below boat ramp	Minimum
AA5639?	3096	73	CRD	89APR502W	1	100 m upstream of boat ramp	Minimum
CAMS-16576	3060	60	CRD	93APR23L	1	Alaganic Slough 1.4km above boat ramp	Minimum
Phase boundary							
Beta-184329	3040	40	Gw	G/03/4P#20	2	Upper boundary of Girdwood peat A	Maximum
Beta-223766	3020	40	Gw	GW5/3	2	Upper boundary of Girdwood peat A	Maximum
Beta-223763	3010	40	Gw	GW1/1	2	Upper boundary of Girdwood peat A	Maximum
Beta-223767	2930	40	Gw	GW6/1	2	Upper boundary of Girdwood peat A	Maximum
Earthquake 5							
W6547	3070	50	CRD	93APR21AA	1	Alaganic Slough 0.5km below boat ramp	Minimum
Phase boundary							
AA4905	2855	95	CRD	89APR503J	1	Upper Alaganic Slough	Maximum
AA5637	2662	67	CRD	89APR502O	1	100 m upstream of boat ramp	Maximum
Beta-266422	2580	20	BP	BP/09/1/3	3	Top of Bird Point peat D	Maximum
Beta-184327	2560	40	Gw	G/03/4P#18	2	Top of Girdwood peat D	Maximum
Beta-223768	2490	40	Gw	GW6/2	2	Top of Girdwood peat D	Maximum
CAMS-93961	2425	35	Gw	GW/02/1C#5	2	Top of Girdwood peat D	Maximum
Earthquake 4							
AA5644	2614	89	CRD	89APR503I	1	Upper Alaganic Slough	Minimum
AA5636	2614	65	CRD	89APR502M	1	100 m upstream of boat ramp	Minimum
CAMS-16574	2570	60	CRD	93APR21W	1	Alaganic Slough 0.5km below boat ramp	Minimum
W6452	2550	90	CRD	91APR606H	1	Upper Alaganic Slough redrill	Minimum
Beta - 316250	2390	30	Kat	KR11-3-81	new	Base of peat layer	Minimum
Beta - 328272	2370	40	PS	PF/07/4 - 374	new	Puffy Slough 4 - base of lowest peat	Minimum
AA4892	2342	78	CRD	89APR503G	1	Upper Alaganic Slough	Minimum
Phase boundary							
Beta-266421	2170	20	BP	BP/09/1/2	2	Top of Bird Point peat E	Maximum
AA-48170	2140	47	Gw	GW1A-20	2	Top of Girdwood peat E	Maximum
Beta-184324	2120	50	Gw	G/03/3#15	2	Top of Girdwood peat E	Maximum
Beta-266423	2040	20	Hope	HP/09/8	3	Top of Hope fourth peat (E)	Maximum
Earthquake 3							

Beta - 328270	2120	30	PS	PF/07/4 - 260	new	Puffy Slough 4 - base of middle peat	Minimum
Beta - 316248	2060	30	Kat	KR11-3-51	new	Base of peat layer	Minimum
Beta - 316247	2030	30	Kat	KR11-3-50	new	1cm above base of peat layer	Minimum
Beta-266418	2020	20	CRD	AS/09/5	1	Bottom of Alaganic Slough peat 3	Minimum
AA4890	1882	72	CRD	89APR503F	1	Upper Alaganic Slough	Minimum
Phase boundary							
Beta-184332	1670	40	Ke	KE/03/5#23	4	Top of Kenai peat A	Maximum
CAMS-93964	1670	45	Ke	KE/2000/7#8	4	Top of Kenai peat A	Maximum
W6085	1610	220	CRD	88APR11B	1	Pete Dahl Cutoff	Maximum
Beta-266420	1580	20	BP	BP/09/1/1	3	Top of Bird Point peat F	Maximum
CAMS-93966	1570	35	Kas	KS/01/1#10	5	Top of Kasilof lowest peat	Maximum
Beta-184326	1540	40	Gw	G/03/2#17	2	Top of Girdwood peat F	Maximum
Beta-184318	1530	40	Anc	OV/02/2#9	6	Top of Ocean View peat C	Maximum
Beta-184311	1500	40	Anc	OV/03/23#2	6	Top of Ocean View peat C	Maximum
Earthquake 2							
Beta-223761	1610	40	CRD	AS1/3	new	Bottom boundary of peat 'A'	Minimum
W6361	1540	60	CRD	91APR609J	1	Upper Alaganic Slough	Minimum
Beta - 316245	1510	30	Kat	KR11-1-381	new	Stems within silt layer, above sand	Minimum
W6088	1500	160	CRD	88APR11 C	1	Pete Dahl Cutoff	Minimum
Beta-266416	1480	20	CRD	AS/09/3/2	1	Bottom of Alaganic Slough peat 2	Minimum
W6454	1480	80	CRD	91APR606C	1	Upper Alaganic Slough redrill	Minimum
AA4897	1451	49	CRD	89APR503D	1	Upper Alaganic Slough	Minimum
AA4893	1446	56	CRD	89APR502F	1	100 m upstream of boat ramp	Minimum
Beta-266419	1430	20	CRD	AS/09/8	new	Bottom of Alaganic Slough peat 2	Minimum
Phase boundary							
Beta - 316256	1130	30	Kat	KR11-6-127	new	Within silt layer, below peat contact	Maximum
Beta-184315	1070	40	Anc	OV/01/1B#6	6	Top of Ocean View peat D	Maximum
SUERC-22676	1060	37	BP	BP086R12	3	Top of Bird Point peat G	Maximum
AA5624	998	56	CRD	88APR13AA	new	Lower Pete Dahl Slough	Maximum
SUERC-22673	991	35	BP	BP086R11	3	Top of Bird Point peat G	Maximum
W6098	960	120	CRD	88APR11H	1	Pete Dahl Cutoff	Maximum
CAMS-93958	955	40	Gw	GW/02/1B#2	2	Top of Girdwood peat G	Maximum
Beta-45199	940	60	Gw	GW91-4-1	2	Rooted wood at top of Girdwood peat G	Maximum
Beta-184317	940	50	Anc	OV/03/25#8	6	Top of Ocean View peat D	Maximum
Beta-184321	890	40	Gw	G/03/1#12	2	Top of Girdwood peat G	Maximum

Beta-45197	860	60	Gw	GW91-2-1	2	Rooted wood at top of Girdwood peat G	Maximum
Earthquake 1							
Beta - 212211	970	40	CS	CS 05/2 268cm	7	herbaceous roots/stems, base of peat	Minimum
Beta-242795	970	20	Ya	YK/5-2	8	herbaceous roots/stems, base of peat	Minimum
Beta - 316253	950	30	Kat	KR11-5-97	new	herbaceous roots/stems, base of peat	Minimum
Beta-266417	930	20	CRD	AS/09/4	new	Bottom of Alaganic Slough peat 1	Minimum
Beta - 212213	920	40	CS	CS 05 2 269cm	7	Plant fragment in 1 cm sand below peat layer	Minimum
Beta-239243	920	20	Ya	YK/2	8	herbaceous roots/stems, base of peat	Minimum
Beta-239245	920	20	Ya	YK/5-1	8	herbaceous roots/stems, 3 cm above base of peat	Minimum
M2873	895	50	CRD	89APR505H rer	1	Tiedemann Slough	Minimum
Beta-266415	880	20	CRD	AS/09/3/1	new	Bottom of Alaganic Slough peat 1	Minimum
Beta - 212212	880	40	CS	CS 05/2 266cm	7	herbaceous roots/stems, 2cm above base of peat	Minimum
Beta - 316254	880	30	Kat	KR11-6-122	new	2cm above base of peat layer	Minimum
M2874	865	45	CRD	89APR505H	1	Tiedemann Slough	Minimum
W6123	850	120	CRD	88APR13B	1	Lower Pete Dahl Slough	Minimum
Beta - 316255	840	30	Kat	KR11-6-124	new	herbaceous roots/stems, base of peat	Minimum
Beta-239239	840	20	PS	Puffy_Slough	new	herbaceous roots/stems, base of peat	Minimum
W6102	830	120	CRD	88APR11I	1	Pete Dahl Cutoff	Minimum
Beta - 316252	830	30	Kat	KR11-5-96	new	1cm above base of peat layer	Minimum
Beta - 316260	800	30	Kat	KR11-10-115	new	herbaceous roots/stems, base of peat	Minimum
Beta - 316259	790	30	Kat	KR11-10-113	new	2cm above base of peat layer	Minimum
Beta - 328268	790	30	PS	PF/07/4 - 153	new	Puffy Slough 4 - base of upper peat	Minimum
AA5626	706	54	CRD	88APR16A	1	Alaganic Slough boat ramp	Minimum
Beta-223760	700	40	CRD	AS1/2	new	Bottom boundary of peat 'B'	Minimum
W6139	630	140	CRD	88APR16C	1	Alaganic Slough boat ramp	Minimum
Earthquake 0.5							
Beta - 239238	530	40	Kat	KA/07/4/71	new	herbaceous roots/stems, base of peat	Minimum
Beta - 239237	400	40	Kat	KA/07A/1/45	new	herbaceous roots/stems, base of peat	Minimum
Beta - 318154	270	30	Kat	KR-07B-1-42	new	Herbaceous leaf/stem fragments	Minimum